Styrylpyrimidine chromophores with bulky electron-donating substituents: experimental and theoretical investigation

Maxime Hodée, Julien Massue, Sylvain Achelle, Arnaud Fihey, Denis Tondelier, Gilles Ulrich, Françoise Robin Le Guen, Claudine Katan

M. Hodée et al., Physical Chemistry Chemical Physics, 2023, DOI: 10.1039/D3CP03705C

Styrylpyrimidine chromophores with bulky electron-donating substituents: experimental and theoretical investigation

Maxime Hodée,[a] Julien Massue,[b]* Sylvain Achelle,[a]* Arnaud Fihey,[a]* Denis Tondelier,[c,d] Gilles Ulrich,[b] Françoise Robin-le Guen[a] and Claudine Katan,[a]

[a] Univ Rennes, ENSCR, CNRS, ISCR (Institut des Sciences Chimiques de Rennes) - UMR 6226, F-35000 Rennes, France. E-mails: sylvain.achelle@univ-rennes1.fr, arnaud.fihey@univ-rennes1.fr

[b] Institut de Chimie et Procédés pour l'Energie, l'Environnement et la Santé (ICPEES), UMR CNRS 7515, Equipe Chimie Organique pour la Biologie, les Matériaux et l'Optique (COMBO) 25 Rue Becquerel, 67087 Strasbourg, Cedex 02, France E-mail: massue@unistra.fr

[c] Laboratoire de Physique des Interfaces et des Couches Minces (LPICM), CNRS, Ecole Polytechnique, IP Paris, Palaiseau Cedex, France

[d] Université Paris-Saclay, CEA, CNRS, NIMBE, LICSEN, Gif-sur-Yvette, France

TOC

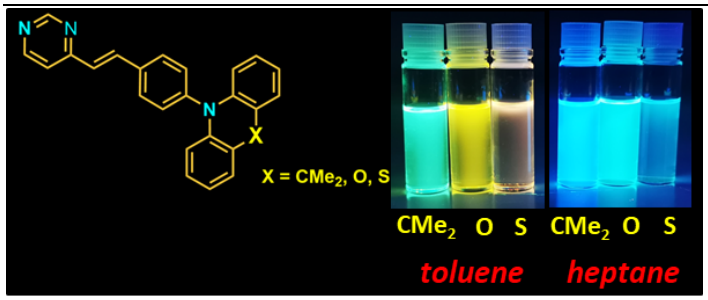

Abstract

Styrylpyrimidine with bulky 9,9-dimethylacridan, phenoxazine and phenothiazine electron-donating fragment were designed. These chromophores exhibit peculiar emission properties. For 9,9-dimethylacridan and phenoxazine derivatives, a single emission highly sensitive to the polarity is observed in solution whereas for phenothiazine derivative a dual emission is observed in solution and is attributed to the coexistence of *quasi-axial* (*Qax*) and *quasi-equatorial* (*Qeq*) conformers. The absence of phosphorescence both at room temperature and 77K tends to indicate the impossibility to harvest triplet states in these systems. Wave-function based calculations show that for both conformers of the three chromophores the S_1-T_1 splitting is significantly larger than 0.2 eV. The second triplet state T_2 of *Qeq* conformers is found very close in energy to the singlet S_1 state, but S_1 and T_2 states possess similar charge transfer characters. This prevents efficient spin-orbit coupling between the states, which is consistent with the absence of thermally activated delayed fluorescence.

Keywords: Pyrimidine, Fluorescence, TD-DFT, Push-Pull

Introduction

Styrylpyrimidine derivatives with electron-donating groups have been extensively studied in the last two decades as push-pull chromophores.[1] This family of chromophores encompasses in particular linear 4-styrylpyrimidines,[2] V-shaped quadrupolar 4,6-distyrylpyrimidines[2a,3], tripodal 2,4,6-tristyrylpyrimidines[4] and other arylvinylpyrimidines.[5] Many of these compounds exhibit photoluminescence properties that can be tuned by external stimuli such as polarity or pH.[2–4,6] Styrylpyrimidines have found a large variety of applications ranging from fluorescent (bio)sensors (metal cations,[7] nitroaromatics,[8] β-amyloid plaques,[9] double-stranded DNA[10] ….), panchromatic white light emission,[11] luminescent liquid crystals,[12] two-photon absorption chromophores for bioimaging,[13] 3D data storage[14] or microfabrication,[15] dyes for dye-sensitized solar cells[16] as well as second order nonlinear optical chromophores for second harmonic generation.[2b,17]

In recent years, thermally activated delayed fluorescence (TADF) chromophores have been subject to intensive research due to their application as emitters for organic light emitting diodes (OLEDs).[18] The pioneer work of Adachi,[19] based on pure organic compounds displaying TADF has emerged as a cutting-edge technology to achieve 100% internal quantum efficiency (IQE) and high external quantum efficiency (EQE), paving the way for a third generation of OLEDs. In addition to high stability and luminance efficiency, metal-free TADF emitters allow the production of a stable deep-blue light, which has always been problematic for previous generations of OLEDs.[20] In addition, TADF chromophores have also found applications in photocatalysis[21] and biomedical applications.[22,23]

The TADF process involves the population of a triplet state after electrical charge injection, followed by the thermally activated conversion to a singlet state by reverse intersystem crossing (RISC) (Figure 1).[24] The involvement of metastable triplet state in the TADF process induces longer fluorescence lifetimes, typically in the microsecond range but the spectral distribution of the emitted light is identical to prompt fluorescence.[18a]

In order to observe TADF, it is necessary to combine an emissive singlet excited state S_1, a sufficiently stable triplet excited state (e.g. T_1) and a small singlet-triplet energy splitting (ΔE_{ST}) generally around 0.1 eV.[18b,20b,25,26] In the case of donor-acceptor compounds, TADF is favored when the spin-orbit coupling is sizeable, which is the case when the singlet excited state exhibit a charge transfer character (^{1}CT) and the triplet corresponds to a local exciton (^{3}LE).[6,27,28,29] Small energy difference between ^{3}LE and ^{1}CT (ΔE_{ST}) will increase the thermally activated upconversion.[30]

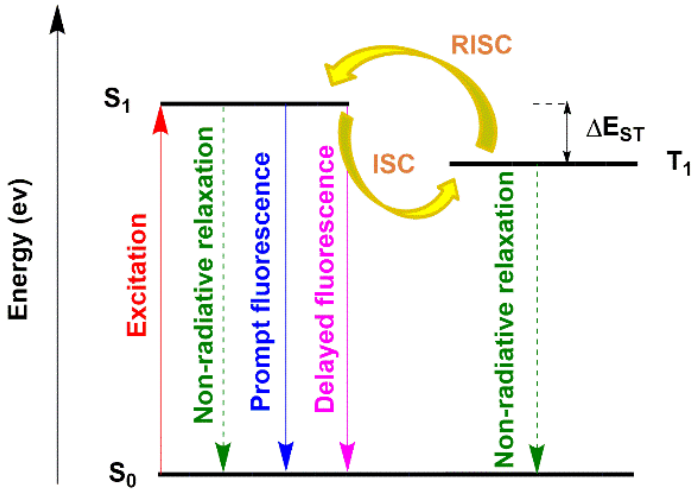

Figure 1. Principle of TADF

For all organic TADF chromophores, the typical design constists in push-pull chromophores with twist/spiro/bulky[31] connection between donor (D) and acceptor (A) parts, permitting to reduce the overlap between the HOMO and LUMO orbitals.[18a,32] Indeed, spatially separated HOMO and LUMO orbitals are required to observe sufficiently small ΔE_{ST} values.[33] Recently, after the pioneer work of Kido and Sasabe,[34] numerous pyrimidine based TADF emitters have been described for OLED applications with high EQE values.[35] In all cases, bulky amino electron-donating groups such as carbazole,[36] 9,9-dimethylacridan,[37] 9,9-diphenylacridan,[38] phenoxazine[39] or phenothiazine[40] are used. Some typical structures are presented in Figure 2. To the best of our knowledge, in all these examples, phenylene unit have been almost always used as π-linker between the pyrimidine core and the electron-donating fragments.

In the course of designing organic chromophores for OLEDs applications, and in particular for TADF applications, Density Functional Theory (DFT) and its Time Dependent variant (TD-DFT) have demonstrated their usefulness in rationalizing structure-properties relationships, and has been successfully used in the case of substituted heterocyclic systems.[41] But, TD-DFT known deficiencies for the treatment of CT electronic transitions or triplet states makes it rather unsuitable to quantitatively predict TADF key properties such as ΔE_{ST}.[41a,42] Wavefunction-based methodologies such as approximate singles and doubles coupled cluster (CC2) [43,44] have recently been used for extended organic systems to study TADF properties.[45] This level of theory proved to be more reliable to investigate the intrinsic nature of the electronic states relevant to the RISC (namely CT and LE)[46] as well as their relative energies.[47] Typically, for the TADF phenomenon to be theoretically expected in organic fluorophores, the singlet-

triplet energy splitting ΔE_{ST} should be smaller than ca. 0.2 eV, and the Spin-Orbit Coupling Matrix Element (SOCME) between these two states should lay around 1 cm^{-1}.[18b,48]

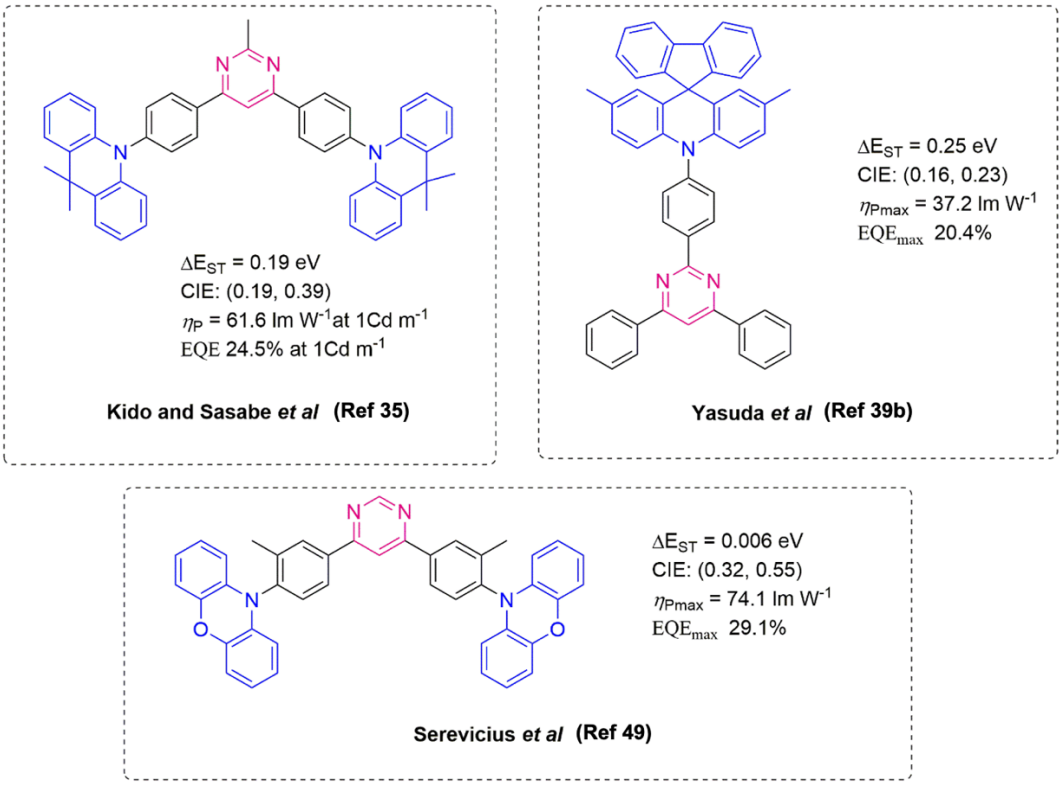

Figure 2. Examples of TADF pyrimidine chromophores[35,39b,49] with characteristics of corresponding OLED devices.

In this contribution, we designed a series of three 4-styrylpyrimidine derivatives substituted by dimethylacridan, phenoxazine and phenothiazine bulky electron-donating groups. While maintaining an orthogonal conformation between the bulky donor group and the rest of the molecules, the styryl linker is expected to increase intramolecular CT and bathochromically shift the emission spectra with regard to phenylene analogues. With the help of experimental and CC2-based theoretical investigation, the emissive behavior of these derivatives and their potential for TADF properties are discussed.

Results and discussion

Synthesis

The target compound **1-3** were obtained with moderate yields (scheme 1) by Pd-catalyzed Buchwald-Hartwig cross-coupling reaction starting from reported (*E*)-4-bromostyrylpyrimidine[2b] with 9,9-dimethyl-9,10-dihydroacridine, 10*H*-phenoxazine and 10*H*-phenothiazine respectively. The coupling reaction does not alter the *E* stereoisomery of the vinylene linker as evidenced by the characteristic coupling constant (^3J(H-H) ~16 Hz) of the doublet of the hydrogen of the double bond.

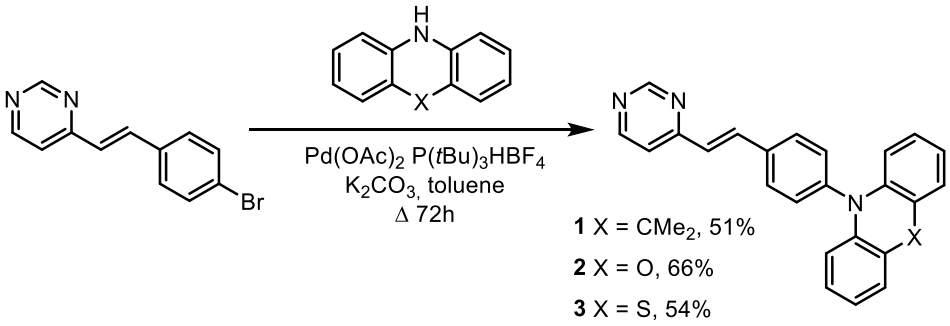

Scheme 1. Synthesis of target compounds **1-3** and corresponding yields.

Photophysical properties

The photophysical properties for styrylpyrimidine derivatives **1-3** were recorded in solution in toluene and *n*-heptane and in the solid-state, as 1% *wt* doped in poly(methyl methacrylate) (PMMA) films at room temperature (298K) and 77K. The photophysical data are compiled in Table 1, while the absorption and emission spectra are displayed on Figure 3.

Table 1. Photophysical data in solution and in the solid-state

Dye	Solvent/ matrix	λ_{abs}[a] (nm)	ε[b] ($M^{-1}.cm^{-1}$)	λ_{em}^{298K}[c] (nm)	λ_{em}^{77K}[d] (nm)	Δss[e] (cm^{-1})	Φ_f[f]	τ^{298K}[g] (ns)	τ^{77K}[h] (ns)
1	toluene	386	2300	512[k]	464[k]	6400	0.12	6.3	4.4/21.0
	heptane	386	2300	441[k]	465[k]	3200	0.10	5.9	5.5/20.0
	PMMA[i]	370[j]	-	473	464	-	0.40	2.8/11.2	2.6/11.0
2	toluene	410	2600	571[l]	507[l]	4700	0.07	5.3	0.7/15.7
	heptane	410	2600	499[l]	507[l]	4700	0.05	4.6	10.6
	PMMA[i]	360[j]	-	514	514	-	0.25	3.4/10.3	3.4/10.2
3	toluene	376	5700	438/584[m]	439[m]	3800	0.02	4.8	1.5
	heptane	376	5700	415/480[m]	446[m]	2500	0.01	0.1/6.1	1.6
	PMMA[i]	360[j]	-	468	452	-	0.14	0.6/4.2	0.5/4.5

[a] Maximum absorption wavelength at 298K, [b] Absorption coefficient at 298 K, [c] Maximum emission wavelength at 298K in deaerated solutions, [d] Maximum emission wavelength at 77K in deaerated solutions, [e] Stokes shift, [f] Relative quantum yield determined in solution at 298K using Rhodamine 6G as a reference (λ_{exc} = 488 nm, Φ = 0.88 in ethanol), [g] lifetime recorded

at 298K, [h] lifetime recorded at 77K, [i] doped in Poly(methylmethacrylate) (PMMA) 1% wt, [j] Excitation wavelength, [k] λ_{exc} = 380 nm, [l] λ_{exc} = 400 nm, [m] λ_{exc} = 375 nm.

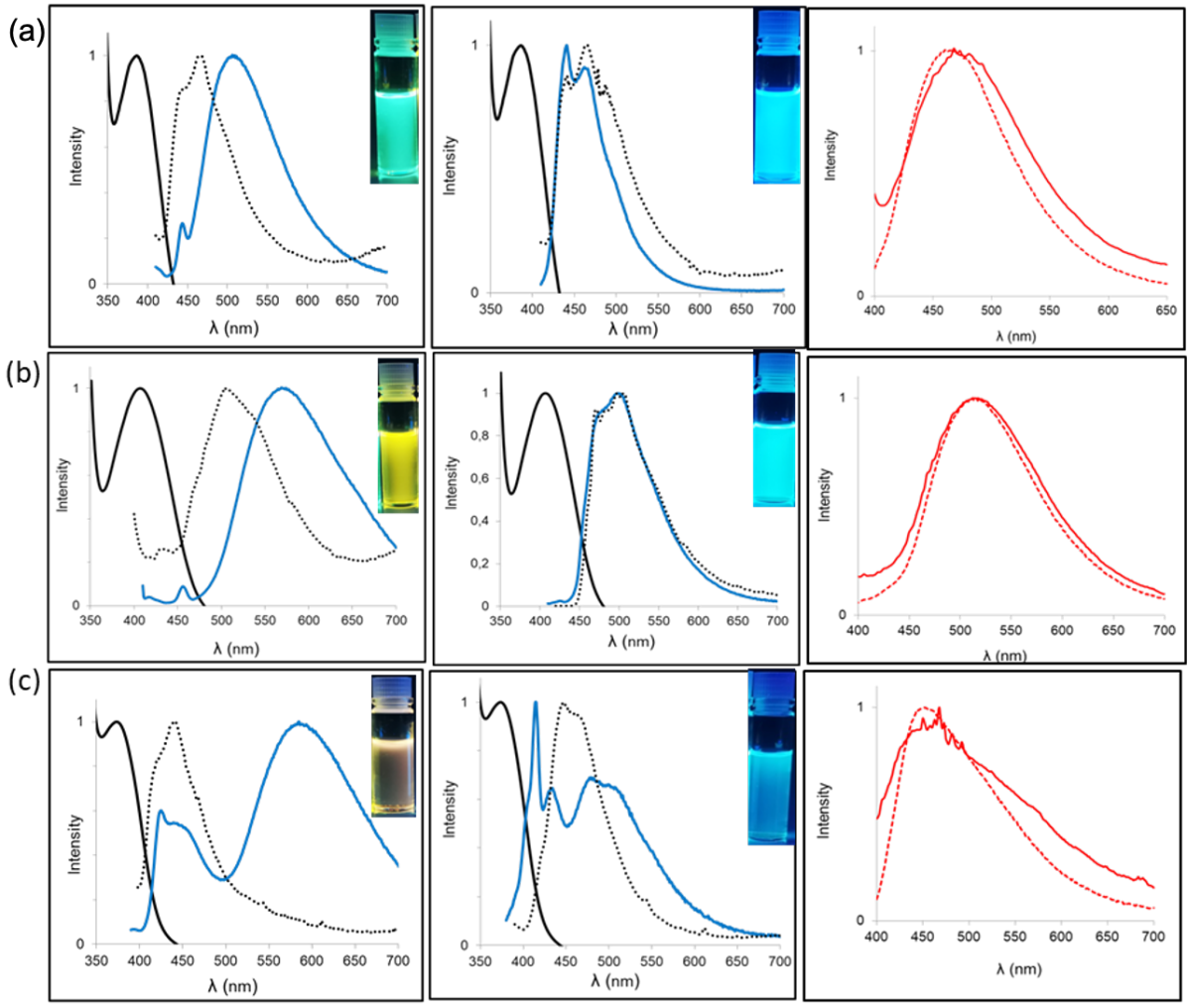

Figure 3. Absorption spectrum (plain black), emission spectra at 298K (blue) and at 77 k (dotted black) in toluene (left) and *n*-heptane (center), emission spectra in PMMA at 298K (plain red) and 77K (dotted red) (right) for dyes (a) **1**, (b) **2** and (c) **3**. Insets: Photographs of solution of dyes **1-3** in toluene and heptane under irradiation using a UV bench lamp (λ_{exc} = 365 nm).

In solution, styrylpyrimidine dyes **1-3** which all show a push-pull structure with sterically hindered donor groups (dimethylacridan, phenoxazine and phenothiazine, respectively) display very similar absorption profiles, *i.e.*, intense bands below 360 nm corresponding to π-π^* transitions (vide infra). Additional weakly intense absorption bands whose maxima peak at 376 nm, 386 nm and 410 nm for **1-3**, respectively are also observed and might be attributed at first sight to CT. The molar absorption coefficients of these bands range

between 2300 and 5700 $M^{-1}.cm^{-1}$. It is interesting to note that phenoxazine substituted dye **2** has the most red-shifted absorption band in the series.

Photoexcitation in the lowest-energy absorption band (370-400 nm) leads to emission in the visible range in both toluene and *n*-heptane for all dyes at room temperature. In toluene, at 298 K, a single emission band is observed for **1** and **2** at 512 and 571 nm, respectively, while for **3** a dual emission is observed (λ_{em} = 438/584 nm). In *n*-heptane, a similar behavior is observed, *i.e.* substituted pyrimidines **1** and **2** display a single emission at 441 and 499 nm, respectively while for **3**, a dual emission is observed (λ_{em} = 415/480 nm). The dual emission might be tentatively attributed to the coexistence of *Quasi-Equatorial* (*Qeq*) and *Quasi-axial* (*Qax*) conformers, as already observed for phenothiazine and dimethylacridan derivatives.[50,51] The position of bands is highly dependent on the nature of the solvent and in particular its dipole moment. Going from toluene to heptane leads to a strong hypsochromic shift from 512 to 441 nm for **1**, from 571 to 499 nm for **2** and from 584 to 480 nm for **3**. It should be mentioned that the dual emission observed for compound **3** is dependent on the excitation wavelength: with excitation at the more energetic absorption band, only one emission band is observed at 586 nm in toluene (Figure S1).

To further study the nature of the emission band, fluorescence was also recorded at 77K for all dyes. In all cases, a single band was observed which was attributed to the decay of the excited ^{1}LE species. In heptane, it is worth mentioning that in the case of **1** and **2**, the emission bands recorded at 298K and 77K are quasi superimposable, which would suggest a similar energy level for ^{1}LE and ^{1}CT in this solvent at room temperature. In toluene, a strong hypsochromic shift occurs for **1** and **2** when freezing the solution, evidencing the sole presence of ^{1}CT at room temperature and ^{1}LE at 77K. The case of **3** seems to be more elusive. In toluene, a single band is observed at 77K, whose maximum emission wavelength is reminiscent to the high energy band at room temperature (λ_{em} = 439 nm vs. 438 nm for **3** at 77K and 298K, respectively). In heptane, however, a significant red-shift is observed for the ^{1}LE at 77K vs. 298K (λ_{em} = 446 nm vs. 415 nm for **3** at 77K and 298K, respectively). It is worth noting that for all dyes studied herein, attempts to record phosphorescence spectra at 298K or 77K remained unsuccessful, highlighting the impossibility to harvest triplet states in these systems.

Emission in the solid-state was also studied for **1-3**, as 1% *wt* doped in PMMA films. The maximum emission wavelengths remained similar, regardless of temperature, and span the range 468-514 nm at 298 K and 452-514 nm at 77K with highly identical shapes.

The luminescent lifetimes, recorded at both temperatures for **1-3** showed on the majority of the cases a dual exponential decay, comprising of a short and a significantly longer value (in

the range of 10 ns), consistent with the short-lived fluorescence of organic dyes and tend to indicate the absence of TADF of these dyes in the specific studied matrixes.

Theoretical study

Among others,[51,51,52] Penfold and co-workers[53] described for phenothiazine-substituted push-pull dyes, the existence of two conformers: *Qeq* and *Qax* (see Figure 4 for a representation). Ground state equilibrium geometries of *Qeq* conformers of **1**, **2** and **3** show a nearly 90° dihedral angle (schematically shown as θ in Figure 4) between the donor group and the styrylpyrimidine acceptor moiety (Table S1). At room temperature, thermal energy is sufficient to induce a change of this angle in the 70°-110° range, as it corresponds to an energy difference of only ca. 2 kcal.mol^{-1} (the corresponding energy profile is plotted in Figure S2). This is expected to influence the D-A character of the ground-state, as well as the CT character of the lowest energy transition.

In their *Qax* conformation, the compounds show a bending angle of the donor unit towards the plane of the styrylpyrimidine moiety (schematically shown as angle ϕ in Figure 4). For both *Qeq* and *Qax*, the phenoxazine and phenothiazine unit in compound **2** and **3**, respectively, exhibits an out of plane conformation, which is more pronounced for the phenothiazine derivative. The styrylpyrimidine moiety itself is in all cases totally planar. Within the series, the *Qeq* and *Qax* conformers appear almost equally stable for **3** (Figure S5), while the *Qeq* is slightly favoured in the case of **1** and **2**, by 1.5 and 3.2 kcal.mol^{-1}, respectively (Figure S3-S4). Energetic barriers of ca. 10 kcal.mol^{-1} are obtained for the three compounds (Figures S3-S5 for a representation of the transition state). Because of their possible coexistence, both *Qeq* and *Qax* conformers will be considered in the following sections.

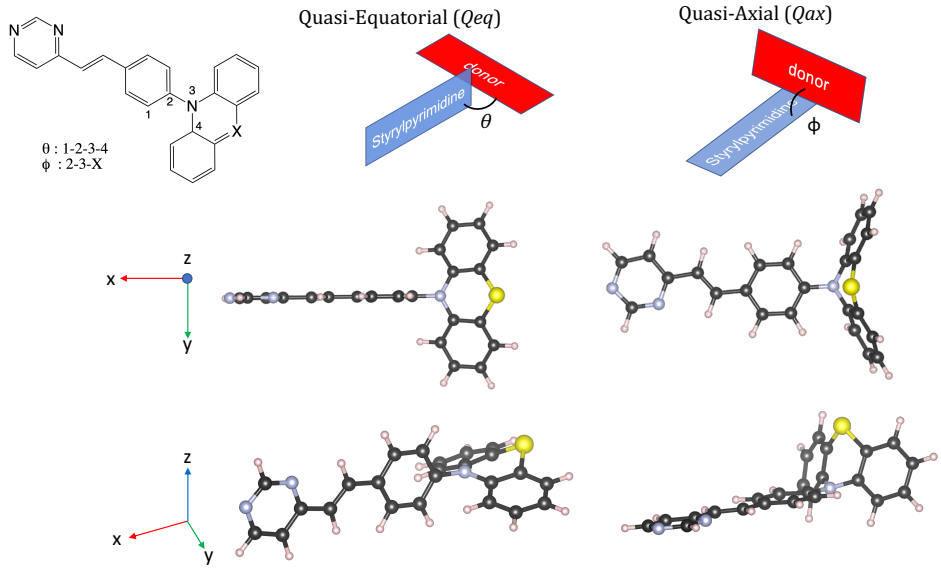

Figure 4: Schematic representation of the *Quasi-equatorial* (*Qeq*) and *Quasi-axial* (*Qax*) conformers, illustrated with the structure of compound **3** in both conformations at the ground state.

From these ground states, the relevant computed excitation energies and oscillator strengths for compounds **1**, **2** and **3** are provided in Table 2. In all cases the *Qeq* conformers present a low energy (S_0 to S_1) transition with a near zero oscillator strength, ranging from 3.07 eV (403 nm) for **1** to 3.33/3.31 eV (372/375 nm) for **2**/**3**. The most intense transition for the *Qeq* conformers that dominates the UV-Visible spectrum is the higher energy S_0 to S_5 transition for **1,** and the S_0 to S_6 transition for **2** and **3**, peaking around 4.20 eV (295 nm). The Natural Transition Orbitals (NTO) plotted in Figure S6 show for each of the *Qeq* conformers a strong charge transfer character of the S_0 to S_1 transition, in agreement with vanishing computed oscillator strength. On the opposite, the NTOs for the S_0 to S_5/S_6 excitation show a clear π–π* localized character on the styrylpyrimidine moiety, explaining the high oscillator strength value computed for these transitions. The *Qax* conformers exhibit different photophysical properties, with intense S_0 to S_1 transitions, peaking between 3.39 eV (366 nm) for **1** and 3.63 eV (341 nm) for **3**. Indeed, in the *Qax* conformation, the orientation between the acridine group and the styrylpyrimidine allows for non-negligible π delocalization along the molecular backbone, thus promoting an intense first π–π* excitation channel (Figure S6).

Theoretically predicted co-existence of both *Qeq* and *Qax* conformers in solution are consistent with the absorption spectra observed experimentally. Indeed, in all three compounds, the intense high energy transition measured in solution can be unambiguously attributed to the S_0 to S_5/S_6 π–π* computed transition of the *Qeq* conformer. Meanwhile, the low energy and lower intensity absorption band may correspond to the S_0 to S_1 excitation of any of the two conformers. In fact, whereas the S_0 to S_1 transition of *Qeq* is computed with a null oscillator strength at equilibrium geometry, it gains sizeable oscillator strength as a result of the above mentioned donor-acceptor angular modulation at finite temperature (θ angle deviating from 90° in Figure 4), especially for compounds **1** and **2** (Table S8). For compound **3**, variation of the dihedral angle hardly increases the oscillator strength, and coexistence of both *Qeq* and *Qax* conformers is likely to be at the origin of the low-energy band in the experimental absorption spectrum (Figure 3).

Table 2: Computed absorption and emission energies (in eV) and wavelengths (in nm) at the SCS-CC2/def2-TZVP level, along with ΔE_{ST} and SOCME between T_1 and S_1 states for *Qeq* and *Qax* conformers in gas phase. See Computational Details section for additional information.

Compound	Conformation	E_{abs} (eV) / λ_{abs} (nm)	f_{abs}	$states_{abs}$	E_{em} (eV) / λ_{em} (nm)	f_{em}	ΔE_{ST} (eV)	SOCME (cm^{-1})
1	*Qeq*	3.07 (404) 4.18 (297)	0 1.38	S_1 S_5	2.64 (470)	0.00	0.49	0.72
	Qax	3.39 (366)	1.35	S_1	3.01 (412)	1.49	0.89	0.06
2	*Qeq*	3.33 (372) 4.19 (296)	0 1.19	S_1 S_6	2.31 (546)	0.00	0.33	0.62
	Qax	3.58 (346)	1.27	S_1	2.98 (406)	1.37	0.92	0.13
3	*Qeq*	3.31 (374) 4.20 (296)	0 1.26	S_1 S_6	2.27 (537)	0.00	0.35	0.18
	Qax	3.63 (341)	1.35	S_1	3.04 (416)	1.37	0.90	0.15

After geometry optimization of the first singlet excited state of each *Qeq* conformer, the donor group becomes more planar, particularly for **3**. The donor part and the styrylpyrimidine groups of **2**/**3** slightly deviate from orthogonality (angle θ), whereas compound **1** does show very limited geometry reorganisation between S_0 and S_1. In the *Qax* conformation, the angle between the donor and the styrylpyrimidine groups (angle ϕ) increases for all compounds, indicating a flattening of the donor group that comes closer to the plan of the acceptor. All the angle values are presented in Table S1. In Table 2 are presented the computed transition energies from the optimized S_1 states to the ground states, quantifying their emission properties. In their *Qeq* conformations, **2** and **3** lead to de-excitation energies of 2.27 (546 nm) and 2.31 eV (536 nm). **1** has a slightly different behaviour with a higher energy at 2.64 eV (470 nm), in line with the smaller reorganization of the molecular structure in the excited state. The lowest lying experimental emission bands recorded at 298K are consistent with the computed data. However, NTOs presented in Figure 5 for **1** (see Figure S7 for **2** and **3**) show that the S_1 to S_0 transition of the *Qeq* conformer has a clear CT character, which leads to near-zero oscillator strengths (Table 2) due to the lack of overlap between orbitals. Thus, if related to *Qeq* conformations, the non-negligible quantum yields experimentally measured at 298K should stem from the conformations deviating from the perfect orthogonal geometry, that may be populated at finite temperature. Experimental data measured for **1** and **2** at 77K, including in PMMA matrixes, remain in line with the computed trends for *Qeq* conformers, but **3** clearly steps out. In parallel, the optimized S_1 states in the *Qax* conformation lead to higher computed de-excitation energies that are found similar for all three compounds, at ca. 3 eV (410 - 415 nm), and bear significant oscillator strength (Table 2). This is related to the delocalized π-π* character of the transition as illustrated for compound **1** in Figure 5 (Figure S7 for **2** and **3**). From the dual emission

observed for **3** in toluene and heptane, as well as the good energy match with the higher lying band observed at room temperature and the single emission line recorded at 77K, or in a PMMA matrix, we assign this higher lying emission band to the LE state of the *Qax* conformer. In short, the observed LE and CT experimental bands in the dual emission of **3** may arise from the presence of both *Qeq* (CT, low energy emission) and *Qax* (LE, high energy emission) conformers. For **1** and **2**, comparison between experimental and computed data suggests that the emission may stem from *Qeq* conformers deviating from perfect orthogonal conformations, leading to reduced CT character and in turn non-zero oscillator strength.

The geometry of the first triplet state of **1**-**3** (*E*)-styrylpyrimidines are found similar to the ground state one (see angles for *Qeq* and *Qax* conformers in Table S1). The NTOs describing the T_1 to S_0 transition show a strong localized character with extended overlap between hole and particle, as illustrated for compound **1** in Figure 5. Table 2 reports the ΔE_{ST} and SOCME values for *Qeq* conformers. For the three compounds, SOCME values are typical of TADF compounds, ranging between 0.18 cm^{-1} and 0.72 cm^{-1}. But, the kinetic rate constant of reverse intersystem crossing and the likelihood of such mechanism also depends on the value of ΔE_{ST}. Here, in all cases, the S_0-T_1 splitting is larger than 0.2 eV; 0.46 eV, 0.33 eV and 0.35 eV for the *Qeq* conformer of **1**, **2** and **3,** respectively. For *Qax* conformers, the triplet is found significantly higher in energy leading to large ΔE_{ST} values, around 0.9 eV. These values are not in favor of any RISC from the T_1 triplet. The second triplet state, T_2, of *Qeq* conformers is found very close in energy to the singlet S_1 state, respectively at 0.025 eV and 0.005 eV above for **1** and **2**, and 0.013 eV below for **3**. However, the S_1 and T_2 states possess a very similar CT nature as illustrated for compound **1** in Figure 5, ruling out any efficient coupling. These theoretical results suggest that TADF is mostly unlikely in these series of styrylpyrimidine based chromophores, in line with experimental findings.

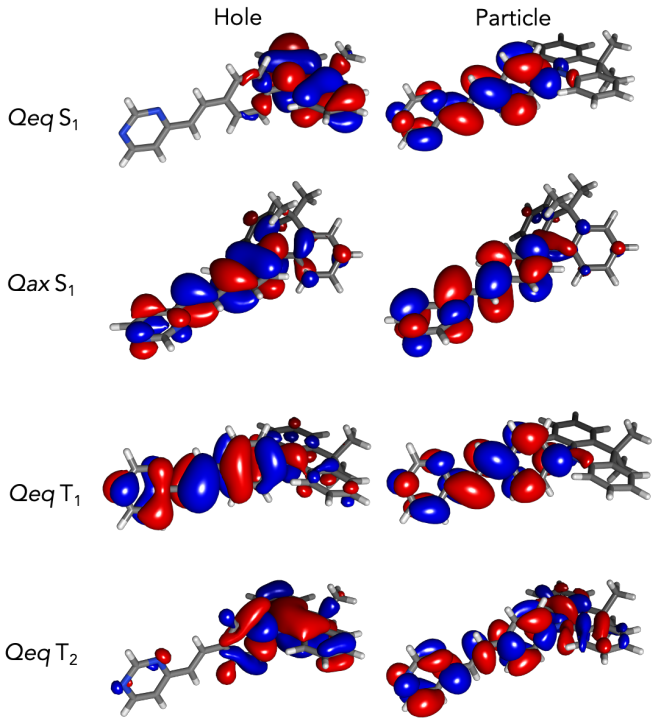

Figure 5: NTOs computed for compounds **1** at the S_1 geometry of *Qeq* and *Qax* conformers, at the T_1 and T_2 geometries of *Qeq* conformer (isovalue = 0.02).

Conclusions

In this work we have investigated the photophysical properties of original push-pull chromophores consisting of styrylpyrimidine functionalized with bulky 9,9-dimethylacridan, phenoxazine and phenothiazine electron-donating fragments. Their potential as TADF emitters has been carefully evaluated both from an experimental and theoretical perspective. No evidence of TADF nor phosphorescence was observed. The phenothiazine derivative shows dual emission, with a low-energy band tentatively attributed to a CT transition of the *Qeq* conformer and a high-energy band related to a LE transition of the *Qax* conformer. For dimethylacridan and phenoxazine derivatives, the comparison between experimental and computed data suggests that the emission may stem from the *Qeq* conformers only, thanks to imperfect orthogonal conformation that reduces the CT character and increases oscillator strength of the transition. S_1-T_1 energy splittings are found significantly larger than 0.2 eV, which is not in favor of TADF. This is not the case for the second triplet state T_2 of *Qeq*

conformers, which is almost isoenergetic with S_1. Nevertheless, both bear a similar CT character, leading to poor spin-orbit coupling, which is also unfavourable to TADF.

Experimental and computational details

General information

All solvents were reagent grade for synthesis. Starting materials were purchased from Sigma-Aldrich or TCI and were used without further purification. Thin layer chromatography (TLC) was conducted on pre-coated aluminum sheets with 0.20 mm Merck Alugram SIL G/UV254 with fluorescent indicator UV254 and 0.25 mm Merck silica gel (60-F254). Column chromatography was carried out using Acros silica gel 60 (particle size 63-200 μm). NMR spectra were recorded in $CDCl_3$ on a Bruker AC-300 spectrometer. The chemical shifts δ are reported in ppm and are referenced to the appropriate solvent signals of $CDCl_3$ (^{1}H, δ = 7.27 ppm; ^{13}C, δ = 77.0 ppm) or DMSO-d_6 (^{1}H, δ = 2.50 ppm; ^{13}C, δ = 39.5 ppm). The coupling constants *J* are given in Hz. In the ^{1}H NMR spectra, the following abbreviations are used to describe the peak patterns: s (singlet), d (doublet), t (triplet), q (quadruplet), m (multiplet). Acidic impurities in $CDCl_3$ were removed by treatment with solid K_2CO_3. High-resolution mass analyses were carried out at the 'Centre Régional de Mesures Physiques de l'Ouest' (CRMPO, Université de Rennes 1) using a Bruker MicroTOF-Q II instrument.

Synthesis

General Procedure for Buchwald Cross-Coupling Reactions : A stirred mixture of (*E*)-4-bromostyrylpyrimidine (261 mg, 1 mmol), secondary amine (1.1 mmol) and potassium carbonate (414 mg, 3 mmol) in degassed toluene (5 mL) was stirred under nitrogen atmosphere for 30 min before addition of the catalyst $Pd(OAc)_2$ (23 mg, 0.1 mmol) and the ligand $P(^tBu)_3HBF_4$ (32 mg, 0.12 mmol). The reaction mixture was then heated to reflux under nitrogen for 72 h in a Schlenk tube. The reaction mixture was cooled, filtered, and dissolved with a 1:1 mixture of CH_2Cl_2 and water (50 mL) and the organic layer was separated. The aqueous layer was extracted with CH_2Cl_2 (2 × 25 mL). The organic phases were combined, dried and evaporated. The residue was purified by column chromatography (SiO_2, AcOEt/petroleum ether, 1:1) followed by recrystallization from DCM/*n*-heptane

(E)-4-(4-(9,9-Dimethyl-9,10-dihydroacridinyl)styryl)pyrimidine (1) : Pale yellow solid. Yield: 51% (198 mg) ^{1}H NMR (300 MHz, $CDCl_3$) δ 9.14 (s, 1H), 8.64 (d, 1H, ^3J(H-H) = 5.4 Hz), 7.93 (d, 1H, ^3J(H-H) = 15.9 Hz), 7.78 (d, 2H, ^3J(H-H) = 8.7 Hz), 7.39 (dd, 2H, ^3J(H-H) = 7.2 Hz, ^3J(H-H) = 1.5 Hz), 7.32-7.27 (m, 2H), 7.07 (d, 1H, ^3J(H-H) = 15.9 Hz), 6.94-6.84 (m, 4H),

6.25-6.22 (m, 2H), 1.62 (s, 6H). ^{13}C NMR (75 MHz, $CDCl_3$) δ 162.0, 159.0, 157.6, 142.4, 140.7, 136.4, 135.5, 131.8, 130.2, 130.0, 126.6, 126.4, 125.3, 120.8, 118.9, 114.0, 36.0, 31.2. HRMS (ESI/ASAP, TOF) m/z calculated for $C_{27}H_{24}N_3$ $[M+H]^+$ 390.1964 found 390.1964.

(E)-4-(4-(10H-phenoxazin-10-yl)styryl)pyrimidine (2) : Yellow solid. Yield: 66% (240 mg) ^{1}H NMR (300 MHz, $CDCl_3$) δ 9.22 (s, 1H), 8.73 (d, 1H, ^3J(H-H) = 5.1 Hz), 7.98 (d, 1H, ^3J(H-H) = 15.9 Hz), 7.83 (d, 2H, ^3J(H-H) = 8.4 Hz), 7.40 (d, 2H, ^3J(H-H) = 8.4 Hz), 7.36 (d, 1H, ^3J(H-H) = 5.1 Hz), 7.13 (d, 1H, ^3J(H-H) = 15.9 Hz), 6.74-6.59 (m, 6H), 5.99 (dd, 2H, ^3J(H-H) = 7.5 Hz, ^4J(H-H) = 1.2 Hz). ^{13}C NMR (75 MHz, $CDCl_3$) δ 161.8, 159.0, 157.6, 144.0, 140.0, 136.1, 135.8, 134.1, 131.4, 130.2, 126.8, 123.3, 121.6, 118.9, 115.6, 113.3 HRMS (ESI/ASAP, TOF) m/z calculated for $C_{27}H_{17}N_3O$ $[M+H]^+$ 363.1366 found 363.1369

(E)-4-(4-(10H-phenothiazin-10-yl)styryl)pyrimidine (3) : Yellow solid. Yield: 54% (205 mg) ^{1}H NMR (300 MHz, $CDCl_3$) δ 9.20 (s, 1H), 8.71 (d, 1H, ^3J(H-H) = 5.1 Hz), 7.96 (d, 1H, ^3J(H-H) = 15.9 Hz), 7.77 (d, 2H, ^3J(H-H) = 8.4 Hz), 7.38 (d, 2H, ^3J(H-H) = 8.4 Hz), 7.34 (d, 1H, ^3J(H-H) = 5.1 Hz), 7.15-7.07 (m, 3H), 6.98-6.89 (m, 4H), 6.49 (d, 2H, ^3J(H-H) = 7.5 Hz). ^{13}C NMR (75 MHz, $CDCl_3$) δ 162.0, 158.9, 157.5, 143.5, 143.0, 136.4, 134.1, 129.7, 128.3, 127.2, 127.0, 125.9, 123.3, 123.1, 118.8, 118.2 HRMS (ESI/ASAP, TOF) m/z calculated for $C_{27}H_{17}N_3S$ $[M+H]^+$ 379.1138 found 379.1138.

Steady state spectroscopy

Absorption spectra were recorded using a dual-beam grating Schimadzu UV-3000 absorption spectrometer with a quartz cuvette of 1 cm of optical path length. The steady-state fluorescence emission and excitation spectra were recorded by using a Horiba S2 Jobin Yvon Fluoromax 4. All fluorescence and excitation spectra were corrected. Solvents for spectroscopy were spectroscopic grade.

The fluorescence quantum yields (Φ_{exp}) were measured in diluted solution with an absorption value below 0.1 at the excitation wavelength using the following equation:

$$\Phi_{exp} = \Phi_{ref} \frac{I}{I_{ref}} \frac{OD_{ref}}{OD} \frac{\eta^2}{\eta^2_{ref}} \quad (eq\ 1)$$

I is the integral of the corrected emission spectrum, OD is the optical density at the excitation wavelength, and η is the refractive index of the medium. The reference system used was Rhodamine 6G, Φ = 88% in ethanol (λ_{exc} = 488 nm).

Luminescence lifetimes were measured on a Horiba Scientific TCSPC system equipped with a nanoLED 370. Lifetimes were deconvoluted with FS-900 software using a light-scattering solution (LUDOX) for instrument response. The excitation source was a laser diode (λ_{exc} = 320 nm).

The fluorescence emission spectra in the solid-state were recorded, as 1% wt doped in poly(methylmethacrylate) (PMMA) films. The quantum yields were calculated as absolute values, using an integration sphere fitted to the spectrofluorimeter.

Computational methods

Ground and excited singlet and triplet geometries, total electronic energies, corresponding transition (absorption and emission) energies and oscillator strengths presented in the main text were obtained at the CC2 level of theory.[43] CC2 calculations were conducted with the TURBOMOLE 7.5.1 package,[54] using the triple valence def2-TZVP basis set, in gas phase, with the Spin-Component Scaling (SCS) approximation.[44] ΔE_{ST} values presented in this work are obtained by computing the CC2 electronic energy difference between the S_1 and T_1 states in their respective equilibrium geometry[37] in gas phase.

For comparison purposes (see Supporting Information, Tables S2 to S7), DFT and its time-dependent variant (TD-DFT, in the Tamm-Dancoff approximation[55]) were also performed with Gaussian 16.[56] In the specific case of triplet states, B3LYP, M06-2X hybrid functionals, as well as ωB97X-D range-separated hybrid functional were compared to obtain ground and excited (singlet and triplet) states geometries, vibration calculations, vertical absorption and emissions, using the triple valence 6-311+G(d,p) basis set in all cases. All DFT calculations were made in gas phase or with the Linear-Response Polarizable Continuum Model (LR-PCM) of toluene. From the comparison between results obtained in gas phase and toluene, we conclude that solvent effects do not change our conclusions based on more accurate CC2 calculations in gas phase, except for an expected shift of the electronic transition energies.

Energetic barriers between *Qeq* and *Qax* conformers were determined at the TD-DFT ωB97X-D level of theory using *Synchronous Transit-Guided Quasi Newton* (STQN) QST3 method.

SOCME values presented in this work were computed at the TD-DFT level (M06-2X/TZVP) on CC2 T_1 geometries in gas phase. M06-2X functional was preferred in this step as this functional returns the closest transition energies values to CC2. These SOCME values were obtained with the ADF software.[57]

Conflicts of interest

There are no conflicts of interest to declare

Acknowledgments

S. A., A. F., C. K. and M. H. are grateful to the EUR LUMOMAT project and the Investments for the Future program ANR-18-EURE-0012. M. H. is thankful to Dr. Manon Bousquet for the frequent discussion on CC2 models.

References

[1] S. Achelle, J. Rodríguez-López and F. Robin-le Guen, *Org. Biomol. Chem.*, 2023, **21**, 39–52.

[2] (a) L. Pascal, J.-J. Vaden Eynde, Y. Van Haverbeke, P. Dubois, A. Michel, U. Rant, E. Zojer, G. Leising, L. O. Van Dorm, N. E. Gruhn, J. Cornil and J.-L. Brédas, *J. Phys. Chem. B*, 2002, **106**, 6442–6450; (b) S. Achelle, A. Barsella, C. Baudequin, B. Caro and F. Robin-le Guen, *J. Org. Chem.,* 2012, **77**, 4087–4096.

[3] S. Achelle, I. Nouira, B. Pfaffinger, Y. Ramondenc, N. Plé and J. Rodríguez-López, *J. Org. Chem.,* 2009, **74**, 3711–3717.

[4] M. Fecková, P. le Poul, F. Robin-le Guen T. Roisnel, O. Pytela, M. Klikar, F. Bureš and S. Achelle, *J. Org. Chem.,* 2018, **83**, 11712–11726.

[5] S. Achelle, J. Rodríguez-López and F. Robin-le Guen, *ChemistrySelect* 2018, **3**, 1852–1886.

[6] A. J. Gillett, A. Pershin, R. Pandya, S. Feldmann, A. J. Sneyd, A. M. Alvertis, E. W. Evans, T. H. Thomas, L.-S. Cui, B. H. Drummond, G. D. Scholes, Y. Olivier, A. Rao, R. H. Friend and D. Beljonne, *Nat. Mater.*, 2022, **21**, 1150–1157.

[7] C. Hadad, S. Achelle, I. López-Solera, J. C. Garía-Martínez and J. Rodríguez-López, *Dyes Pigm.*, 2013, **97**, 230–237.

[8] J.-P. Malval, M. Cranney, S. Achelle, H. Akdas-Kiliç, J.-L. Fillaut, N. Cabon, F. Robin-le Guen, O. Soppera and Y. Molard, *Chem. Commun.*, 2019, **55**, 14331–14334.

[9] A. Boländer, D. Kiesser, C. Voss, S. Bauer, X. Schön, S. Burgold, T. Bittner, J. Hölzer, R. Heyny-von Haußen, G. Mall, V. Goetschy, C. Czech, H. Knust, R. Berger, J. Herms, I. Hilger and B. Schmidt, *J. Med. Chem.*, 2012, **55**, 9170–9180.

[10] A. I. Aranda, S. Achelle, F. Hammerer, F. Mahuteau-Betzer and M.-P. Teulade-Fichou, *Dyes Pigm.*, 2012, **95**, 400–407.

[11] S. Achelle, J. Rodríguez-López, C. Katan and F. Robin-le Guen, *J. Phys. Chem. C*, 2016, **120**, 26986–26995.

[12] H. Akdas-Kiliç, M. Godfroy, J.-L. Fillaut, B. Donnio, B. Heinrich, P. Kedziora, J.-P. Malval, A. Spangenberg, S. Cleuvenbergen, K. Clays and F. Camerel, *J. Phys. Chem. C*, 2015, **119**, 3697–3710.

[13] (a) B. Liu, H.-L. Zhang, J. Liu, Y.-D. Zhao, Q.-M. Luo and Z.-L. Huang, *J. Mater. Chem.*, 2007, **17**, 2921–2929; (b) L. Li, J. Ge, H. Wu, Q.-H. Xu and S. Q. Yao, *J. Am. Chem. Soc.*, 2012, **134**, 12157–12167; (c) L. Hu, S. Husain, T. Liu, Y. Yue, J. Liu, Y. Tian and X. Tian, *New J. Chem.*, 2018, **42**, 14725–14728.

[14] L. Li, Y. Tian, J.-X. Yang, P.-P. Sun, J.-Y. Wu, H.-P. Zhou, S.-Y. Zhang, B.-K. Jin, X.-J. Xing, C.-K. Wang, M. Li, G.-H. Chen, H.-H. Tang, W.-H. Huang, X.-T. Tao and M.-H. Jiang, *Chem. Asian J.*, 2009, **4**, 668–680.

[15] J.-P. Malval, S. Achelle, L. Bodiou, A. Spangenberg, L. C. Gomez, O. Soppera and F. Robin-le Guen, *J. Mater. Chem. C*, 2014, **2**, 7869–7880.

[16] I. Duesto, S. Sarasa, D. Barrios, J. Orduna, B. Villacampa and M.-J. Blesa, *Dyes Pigm.*, 2022, **203**, 110310.

[17] (a) S. van Cleuvenbergen, P. Kedziora, J.-L. Fillaut, T. Verbiest, K. Clays, H. Akdas-Kiliç and F. Camerel, *Angew. Chem. Int.*, *Ed.* 2017, **56**, 9564–9550; (b) R. J. Durand, S. Gauthier, S. Achelle, T. Groazard, S. Kahlal, J.-Y. Saillard, A. Barsella, N. le Poul and F. Robin-le Guen, *Dalton Trans.*, 2018, **47**, 3965–3975.

[18] (*a*) Y. Tao, K. Yuang, T. Chen, P. Xu, H. Li, R. Chen, C. Zheng, L. Zhang and W. Huang *Adv. Mater.*, 2014, **26**, 7631–7958; (*b*) M. Y. Wong and E. Zysman-Colman *Adv. Mater.*, 2017, **29**, 1605444; (*c*) J.6M. Teng, Y.-F. Wang and C.-F. Chen, *J. Mater. Chem. C*, 2020, **8**, 11340–11353; (*d*) W. Che, Y. Xie and Zhen Li *Asian J. Org. Chem.*, 2020, **9**, 1262–1276; (*e*) M. Cai, D. Zhang and L. Duan *Chem. Rec.*, 2019, **19**, 1611–1623.

[19] (*a*) A. Endo, K. Sato, K. Yoshimura, T. Kai, A. Kawada, H. Miyazaki and C. Adachi *Appl. Phys. Lett.*, 2011, **98**, 083302; (*b*) H. Uoyama, K. Goushi, K. Shizu, H. Nomura and C. Adachi *Nature*, 2012, **492**, 234–238; (*c*) Q. Zhang, B. Li, S. Huang, H. Nomura, H. Tanaka and C. Adachi *Nat. Photonics*, 2014, **8**, 326–332.

[20] (*a*) T.-T. Bui, F. Goubard, M. Ibrahim-Ouali, D. Gigmes and F. Dumur *Beilstein J. Org. Chem.*, 2018, **14**, 282–308; (*b*) S. Scholz, D. Kondakov, B. Lüssem and K. Leo *Chem. Rev.*, 2015, **115**, 8449–8503.

[21] M. A. Bryden and E. Zysman-Colman *Chem. Soc. Rev.*, 2021, ***50***, 7587–7680.

[22] V.-N. Nguyen, A. Kumar, M. H. Lee and J. Yoon *Coord. Chem. Rev.*, 2020, **425**, 213545.

[23] W. Liu, C. Zhang, R. Alessandri, B. T. Diroll, Y. Li, H. Liang, X. Fan, K. Wang, H. Cho, Y. Liu, Y. Dai, Q. Su, N. Li, S. Li, S. Wai, Q. Li, S. Shao, L. Wang, J. Xu, X. Zhang, D. V. Talapin, J. J. De Pablo and S. Wang, *Nat. Mater.*, 2023, **22**, 737–745.

[24] P. Pander and F. B. Dias *Display Imaging*, 2017, **2**, 249–263.

[25] (*a*) L. Gan, K. Gao, X. Cai, D. Chen, S. J. Su, *J. Phys. Chem. Lett.*, 2018, **9**, 4725–4731; (*b*) P. L. Santos, J. S. Ward, P. Data, A. S. Bartsanov, M. R. Bryce, F. B. Dias, A. P. Monkman, *J. Mater. Chem. C*, 2016, **4**, 3815–3824.

[26] N. Aizawa, Y.-J. Pu, Y. Harabuchi, A. Nihonyanagi, R. Ibuka, H. Inuzuka, B. Dhara, Y. Koyama, K. Nakayama, S. Maeda, F. Araoka and D. Miyajima, *Nature*, 2022, **609**, 502–506.

[27] F. B. Dias, K. N. Bourdakos, V. Jankus, K. C. Moss, K. T. Kamtekar, V. Bhalla, J. Santos, M. R. Bryce and A. P. Monkman, *Adv. Mater.*, 2013, **25**, 3707–3714.

[28] Z. Zhao, S. Yan and Z. Ren, *Acc. Chem. Res.*, 2023, **56**, 1942–1952.

[29] J. Li, M. Zhang, T. Li, D. Guo, T. Tian and H. Zhang, *J. Mater. Chem. C*, 2022, **10**, 13124–13136.

[30] (*a*) B. Li, Z. Wang, S.-J. Su, F. Guo, Y. Cao and Y. Zhang, *Adv. Opt. Mater.* 2019, **7**, 1801496; (*b*) M. K. Etherington, J. Gibson, H. F. Higginbotham, T. J. Penfold and A. P. Monkman *Nat. Commun.*, 2016, **7**, 13680; (*c*) F. B. Dias, J. Santos, D. R. Graves, P. Data, R. S. Nobuyasu, M. A. Fox, A. S. Batsanov, T. Palmeira, M. N. Berberan-Santos, M. R. Bryce and A. P. Monkman, *Adv. Sci.*, 2016, **3**, 1600080.

[31] N. Sharma, M. Maciejczyk, D. Hall, W. Li, V. Liégeois, D. Beljonne, Y. Olivier, N. Robertson, I. D. W. Samuel and E. Zysman-Colman, *ACS Appl. Mater. Interfaces*, 2021, **13**, 44628–44640.

[32] (*a*) T. Nakagawa, S. Y. Ku, K. T. Wong and C. Adachi, *Chem. Commun.*, 2012, **48**, 9580–9582; (*b*) G. Mehes, H. Nomura, Q. S. Zhang, T. Nakagawa and C Adachi, *Angew. Chem. Int. Ed.*, 2012, **51**, 11311–11315; (*c*) K. Nasu, T. Nakagawa, H. Nomora, C. Lin, C. Cheng, M. Tseng, T. Yasuda and C. Adachi, *Chem. Commun.*, 2013, **49**, 10385–10387.

[33] (*a*) M. Liu, Y. Seino, D. Chen, S. Inomata, S.-J. Su, H. Sasabe and J. Kido, *Chem. Commun.*, 2015, **51**, 16353–16356; (*b*) Y. Tao, K. Yuan, T. Chen, P. Xu, H. H. Li, R. F. Chen, C. Eheng, L. Zhang and W. Huang, *Adv. Mater.*, 2014, **26**, 7931–7958; (*c*) H. Wang, L. S. Xie, Q. Peng, L. Q. Meng, Y. Wang, Y. P. Yi and P. F. Wang, *Adv. Mater.*, 2014, **26**, 5198–5204.

[34] R. Komatsu, H. Sasabe, Y. Seino, K. Nakao and J. Kido, *J. Mater. Chem. C*, 2016, **4**, 2274–2278.

[35] (*a*) R. Komatsu, H. Sasabe and J. Kido, *J. Photonics Energy*, 2018, **8**, 032108; (*b*) S. Achelle, M. Hodée, J. Massue, A. Fihey, C. Katan, *Dyes Pigm.*, 2022, **200**, 110157; (c) L. Yu, C. Yang, *J. Mater. Chem. C*, 2021, **9**, 17265–17286.

[36] (*a*) M. Cai, D. Zhang, J. Xu, X. Hong, C. Zhao, X. Song, Y. Qiu, H. Kaji and L. Duan *ACS Appl. Mater. Interfaces*, 2019, **11**, 1096–1108; (*b*) J. S. Jang, H. L. Lee, K. H. Lee and J. Y. Lee *J. Mater. Chem. C*, 2019, **7**, 12695–12703; (*c*) T. Serevičius, J. Dodonova, R. Skaisgiris, D. Banevičius, K. Kazlauskas, S. Juršėnas and S. Tumkevičius *J. Mater. Chem. C*, 2020, **8**, 11192–11200.

[37] (a) K.-C. Pan, S.-W. Li, Y.-Y. Ho, Y.-J. Shiu, W.-L. Tsai, M. Jiao, W.-K. Lee, C.-C. Wu, C. L. Chung, T. Chatterjee, Y.-S. Li, K.-T. Wong, H.-C. Hu, C.-C. Chen and M. T. Lee, *Adv. Funct. Mater.* 2016, *26*, 7560–7571; (*b*) K. Nakao, H. Sasabe, R. Komatsu, Y. Hayasaka, T. Ohsawa and J. Kido, *Adv. Opt. Mater.*, 2017, **5**, 1600843.

[38] I. S. Park, J. Lee and T. Yasuda*, J. Mater. Chem. C*, 2016, **4**, 7911–7916.

[39] (a) K. Wu, T. Zhang, L. Zhan, C. Zhong, S. Gong, N. Jiang, Z.-H. Lu and C. Yang, *Chem. Eur. J.*, 2016, **22**, 10860–10866; (*b*) T. Serevičius, R. Skaisgiris, J. Dodonova, L. Jagintavičius, D. Banevičius, K. Kazlauskas, S. Tumkevičius and S. Juršėnas *ACS Appl. Mater. Interfaces*, 2020, *12*, 10727–10736; (c) Y. Xiang, P. Li, S. Gong, Y.-H. Huang, C.-Y. Wang, C. Zhong, W. Zeng, Z. Chen, W.-K. Lee, X. Yin, C.-C. Wu and C. Yang, *Sci Adv.*, 2020, **6**, eaba7855.

[40] T. Serevičius, R. Skaisgiris, J. Dodonova, K. Kazlauskas, S. Juršėnas and S. Tumkevičius *Phys. Chem. Chem. Phys.*, 2020, **22**, 265–272.

[41] (a) Q. Zhu, X. Guo and J. Zhang, *J. Comput. Chem.*, 2019, **40**, 1578–1585; (b) B. Li, Z. Wang, S. Su, F. Guo, Y. Cao and Y. Zhang, *Adv. Opt. Mater.*, 2019, **7**, 1801496.

[42] (a) A. D. Laurent and D. Jacquemin, *Intern. J. Quantum Chem.*, 2013, **113**, 2019–2039; (b) D. Jacquemin, I. Duchemin and X. Blase, *J. Chem. Theory Comput.*, 2015, **11**, 5340–5359.

[43] O. Christiansen, H. Koch and P. Jorgensen, *Chem. Phys. Lett.*, 1995, **243**, 409–418.

[44] A. Hellweg, S. A. Grün and C. Hättig, *Phys. Chem. Chem. Phys.*, 2008, **10**, 4119.

[45] A. Pershin, D. Hall, V. Lemaur, J.-C. Sancho-Garcia, L. Muccioli, E. Zysman-Colman, D. Beljonne and Y. Olivier, *Nat Commun.*, 2019, **10**, 597; (b) D. Hall, S. M. Suresh, P. L. dos Santos, E. Duda, S. Bagnich, A. Pershin, P. Rajamalli, D. B. Cordes, A. M. Z. Slawin, D. Beljonne, A. Köhler, I. D. W. Samuel, Y. Olivier and E. Zysman- Colman, *Adv. Opt. Mater.*, 2020, **8**, 1901627.

[46] P. K. Samanta, D. Kim, V. Coropceanu and J.-L. Brédas, *J. Amer. Chem. Soc.*, 2017, **139**, 4042–4051.

[47] M. A. El- Sayed, *J. Chem. Phys.*, 1963, **38**, 2834–2838.

[48] (a) Y. J. Cho, B. D. Chin, S. K. Jeon and J. Y. Lee, *Adv. Funct. Mater.*, 2015, **25**, 6786–6792; (b) T. Hatakeyama, K. Shiren, K. Nakajima, S. Nomura, S. Nakatsuka, K. Kinoshita, J. Ni, Y. Ono and T. Ikuta, *Adv. Mater.*, 2016, **28**, 2777–2781.

[49] I. S. Park, H. Komiyama and T. Yasuda, *Chem. Sci.,* 2017, **8**, 953–960.

[50] T. Serevičius, R. Skaigiris, J. Dodonova, L. Jagintavičius, J. Bucevičius, K. Kazlauskas, S. Juršėnas and S. Tumkevičius, *Chem. Commun.*, 2019, **55**, 1975–1978.

[51] K. Stavrou, L. G. Franca, T. Böhmer, L. M. Duben, C. M. Marian and A. P. Monkman, *Adv Funct Mater.*, 2023, 2300910.

[52] H. Tanaka, K. Shizu, H. Nakanotani and C. Adachi, *J. Phys. Chem. C*, 2014, **118**, 15985–15994.

[53] T. J. Penfold, F. B. Dias and A. P. Monkman, *Chem. Commun*., 2018, **54**, 3926–3935.

[54] a) S. G. Balasubramani, G. P. Chen, S. Coriani, M. Diedenhofen, M. S. Frank, Y. J. Franzke, F. Furche, R. Grotjahn, M. E. Harding, C. Hättig, A. Hellweg, B. Helmich-Paris, C. Holzer, U. Huniar, M. Kaupp, A. Marefat Khah, S. Karbalaei Khani, T. Müller, F. Mack, B. D. Nguyen, S. M. Parker, E. Perlt, D. Rappoport, K. Reiter, S. Roy, M. Rückert, G. Schmitz, M. Sierka, E. Tapavicza, D. P. Tew, C. van Wüllen, V. K. Voora, F. Weigend, A. Wodyński and J. M. Yu, *J. Chem. Phys.*, 2020, **152**, 184107; b) TURBOMOLE V7.5.1 2021, a development of University of Karlsruhe and Forschungszentrum Karlsruhe GmbH, 1989-2007, TURBOMOLE GmbH, since 2007; available from https://www.turbomole.org.

[55] M. J. G. Peach, M. J. Williamson and D. J. Tozer, J.Chem. Theor. Comput., 2011, **7**, 3578–3585.

[56] Frisch, M. J., Trucks, G. W., Schlegel, H. B., Scuseria, G. E., Robb, M. A., Cheeseman, J. R., Scalmani, G., Barone, V., Petersson, G. A., Nakatsuji, H., Li, X., Caricato, M., Marenich, A. V., Bloino, J., Janesko, B. G., Gomperts, R., Mennucci, B., Hratchian, H. P., Ortiz, J. V., Izmaylov, A. F., Sonnenberg, J. L., Williams, Ding, F., Lipparini, F., Egidi, F., Goings, J., Peng, B., Petrone, A., Henderson, T., Ranasinghe, D., Zakrzewski, V. G., Gao, J., Rega, N., Zheng, G., Liang, W., Hada, M., Ehara, M., Toyota, K., Fukuda, R., Hasegawa, J., Ishida, M., Nakajima, T., Honda, Y., Kitao, O., Nakai, H., Vreven, T., Throssell, K., Montgomery Jr., J., Peralta, J. E., Ogliaro, F., Bearpark, M. J., Heyd, J. J., Brothers, E. N., Kudin, K. N., Staroverov, V. N., Keith, T. A., Kobayashi, R., Normand, J., Raghavachari, K., Rendell, A. P., Burant, J. C., Iyengar, S. S., Tomasi, J., Cossi, M., Millam, J. M., Klene, M., Adamo, C., Cammi, R., Ochterski, J. W., Martin, R. L., Morokuma, K., Farkas, O., Foresman, J. B., and Fox, D. J., Gaussian 16, Revision A.03, Gaussian Inc., Wallingford CT, 2016.

[57] G. te Velde, F. M. Bickelhaupt, E. J. Baerends, C. Fonseca Guerra, S. J. A. van Gisbergen, J. G. Snijders and T. Ziegler, *J. Comput. Chem.*, 2001, **22**, 931–967.

Supporting Information

Table S1: Angles within the **1-3** series for the ground and first singlet/triplet excited states, characterizing the twist between the styrylpyrimidine and acridine groups computed at the SCS-CC2/def2-TZVP level in gas phase. For *Qeq*, we considered the dihedral angle $\widehat{1234}$ called θ and for *Qax* the angle $\widehat{23X}$ called ϕ. Atom numbering is defined in Figure S8.

	1			**2**			**3**		
	S_0	S_1	T_1	S_0	S_1	T_1	S_0	S_1	T_1
$\widehat{1234}$ (θ, *Qeq*)	89°	90°	89°	73°	93°	73°	81°	91°	74°
$\widehat{23X}$ (ϕ, *Qax*)	125°	136°	125°	115°	143°	115°	98°	136°	98°

Table S2: ωB97X-D/6-311+G(d,p) TD-DFT calculations of vertical excitation and de-excitation for both conformers in gas phase.

Conformer	**Cmpd**	E_{abs} (eV)	λ_{abs} (nm)	f_{abs}	$State_{abs}$	E_{em} (eV)	λ_{em} (nm)	f_{em}
Qeq	**1**	4.41	281	1.51	S_3	3.30	375	0.20
	2	4.42	280	1.44	S_4	3.00	413	0
	3	4.42	281	1.49	S_3	3.01	411	0
Qax	**1**	3.83	319	1.54	S_1	3.43	361	1.73
	2	3.98	311	1.50	S_1	3.44	361	1.69
	3	3.98	311	1.50	S_1	3.46	358	1.69

Table S3: M06-2X/6-311+G(d,p) TD-DFT calculations of vertical excitation and de-excitation for both conformers in gas phase.

Conformer	**Cmpd**	E_{abs} (eV)	λ_{abs} (nm)	f_{abs}	$State_{abs}$	E_{em} (eV)	λ_{em} (nm)	f_{em}
Qeq	**1**	4.40	282	1.52	S_4	2.93	423	0
	2	4.41	281	1.46	S_4	2.60	476	0
	3	4.41	281	1.51	S_4	2.55	486	0
Qax	**1**	3.78	328	1.52	S_1	3.38	367	1.73
	2	3.89	319	1.46	S_1	3.37	368	1.65
	3	3.92	316	1.47	S_1	3.41	364	1.67

Table S4: B3LYP/6-311+G(d,p) TD-DFT calculations of vertical excitation and de-excitation for both conformers in gas phase.

Conformer	**Cmpd**	E_{abs} (eV)	λ_{abs} (nm)	f_{abs}	$State_{abs}$	E_{em} (eV)	λ_{em} (nm)	f_{em}
Qeq	**1**	4.01	309	1.49	S_7	1.88	660	0
	2	4.00	310	1.34	S_8	1.52	818	0
	3	4.00	310	1.23	S7	1.46	849	0
Qax	**1**	3.24	383	1.33	S_1	/ [a]	/[a]	/ [a]
	2	3.27	379	1.16	S_1	/[a]	/[a]	/[a]
	3	3.32	374	1.22	S_1	3.25	382	0.16

[a] No stable Qax conformer found

Table S5: ωB97X-D/6-311+G(d,p) TD-DFT calculations of excitation and de-excitation for both conformers in toluene.

Conformer	Cmpd	E_{abs} (eV)	λ_{abs} (nm)	f_{abs}	$State_{abs}$	E_{em} (eV)	λ_{em} (nm)	f_{em}
Qeq	1	4.24	292	1.58	S_2	3.16	392	0.95
	2	4.27	292	1.54	S_4	3.02	410	0.67
	3	4.25	292	1.56	S_3	3.09	401	0.00
Qax	1	3.71	334	1.65	S_1	3.14	395	1.84
	2	3.81	325	1.60	S_1	3.15	394	1.82
	3	3.80	326	1.61	S_1	3.17	391	1.82

Table S6: M06-2X/6-311+G(d,p) TD-DFT calculations of vertical excitation and de-excitation for both conformers in toluene.

Conformer	Cmpd	E_{abs} (eV)	λ_{abs} (nm)	f_{abs}	$State_{abs}$	E_{em} (eV)	λ_{em} (nm)	f_{em}
Qeq	1	4.23	293	1.61	S_2	2.97	418	0.28
	2	4.25	292	1.57	S_3	2.70	460	0.00
	3	4.24	292	1.61	S_3	2.65	467	0.00
Qax	1	3.60	344	1.64	S_1	3.09	401	1.88
	2	3.71	334	1.58	S_1	3.10	400	1.84
	3	3.73	332	1.58	S_1	3.13	396	1.84

Table S7: B3LYP/6-311+G(d,p) TD-DFT calculations of vertical excitation and de-excitation for both conformers in toluene.

Conformer	Cmpd	E_{abs} (eV)	λ_{abs} (nm)	f_{abs}	$State_{abs}$	E_{em} (eV)	λ_{em} (nm)	f_{em}
Qeq	1	3.82	324	1.59	S_5	1.93	642	0.00
	2	3.84	323	1.54	S_7	1.61	770	0.00
	3	3.82	324	1.56	S_5	1.56	794	0.00
Qax	1	3.03	409	1.46	S_1	2.82	440	1.54
	2	3.08	402	1.31	S_1	/[a]	/[a]	/[a]
	3	3.12	397	1.38	S_1	/[a]	/[a]	/[a]

[a] no stable Qax conformer found

Table S8: Transition energies, oscillator strengths and corresponding states involved for different dihedral angles between the styrylpyrimidine and the acridine groups of the Qeq conformer. The dihedral angle is $\widehat{1234}$, with atom numbering defined in Figure S8. Values are computed at the SCS-CC2/def2-TZVP level in gas phase.

	Dihedral Angle $\widehat{1234}$ (°)	**E (eV)**	***f***	**States**
1	75	3.05	0.11	$S_0 \rightarrow S_1$
		4.10	0.12	$S_0 \rightarrow S_3$
		4.21	1.16	$S_0 \rightarrow S_4$
		4.39	0.25	$S_0 \rightarrow S_5$
	105	3.05	0.08	$S_0 \rightarrow S_1$
		4.10	0.11	$S_0 \rightarrow S_3$
		4.20	1.20	$S_0 \rightarrow S_4$
		4.39	0.53	$S_0 \rightarrow S_5$
2	75	3.10	0.17	$S_0 \rightarrow S_1$
		4.13	0.11	$S_0 \rightarrow S_4$
		4.24	1.13	$S_0 \rightarrow S_5$
	105	3.10	0.07	$S_0 \rightarrow S_1$
		4.16	0.13	$S_0 \rightarrow S_4$
		4.21	1.15	$S_0 \rightarrow S_5$
3	75	3.28	0.01	$S_0 \rightarrow S_1$
		4.17	0.23	$S_0 \rightarrow S_4$
	105	3.28	0.01	$S_0 \rightarrow S_1$
		4.17	0.28	$S_0 \rightarrow S_4$

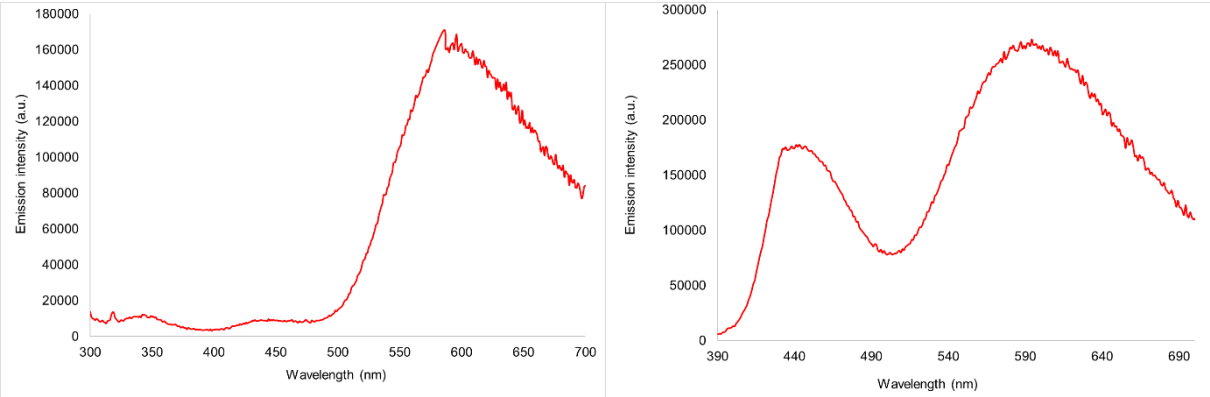

Figure S1: Emission spectra of compound **3** in toluene ($c = 1 \times 10^{-5}$ M) after excitation at 290 nm (left) and 380 nm (right)

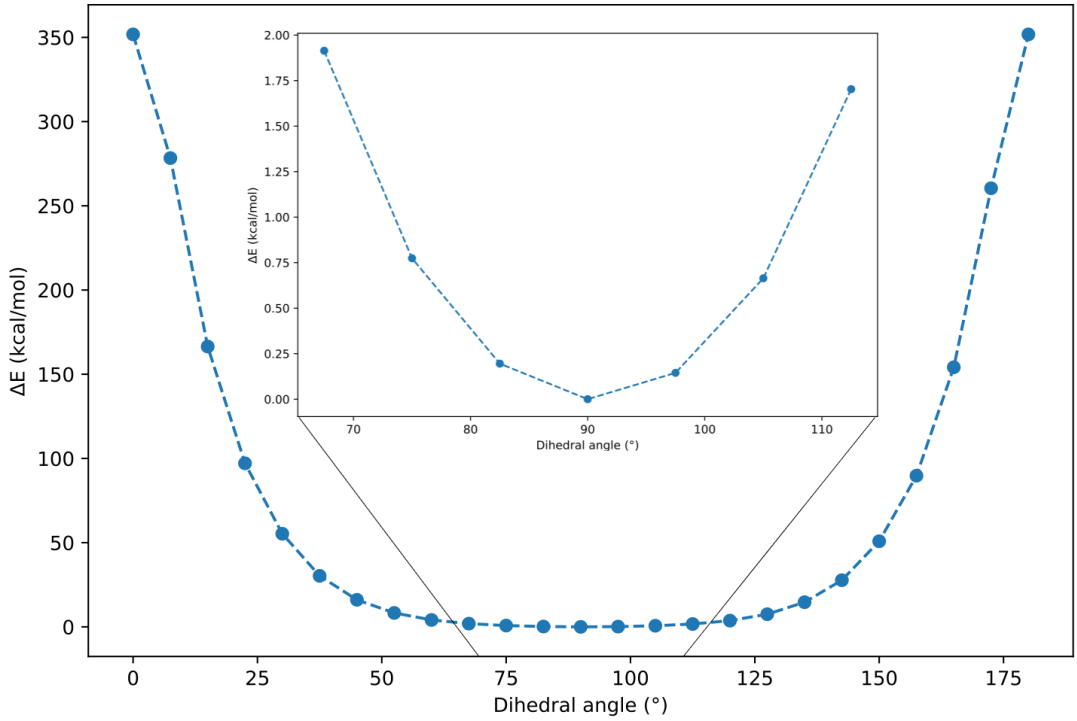

Figure S2: Rigid scan of the ground state of compound **1** along the donor-acceptor θ angle (Figure S8), at the DFT level (ωB97X-D/6-311+G(d,p) (PCM: CH_2Cl_2).

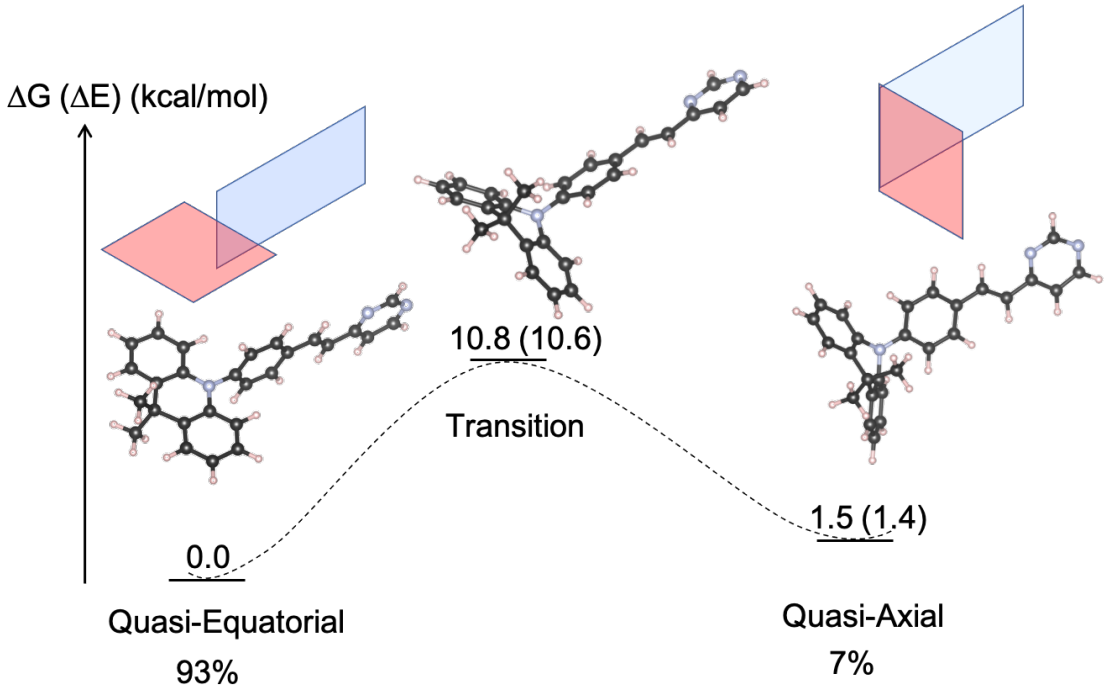

Figure S3: Relative total Gibbs free energies (total electronic energies in parenthesis) of the *Qeq* and *Qax* conformers and of the transition state, obtained at the ωB97X-D/6-311+G(d,p) level of theory for compound **1**. Boltzmann relative populations obtained with ΔG are also presented.

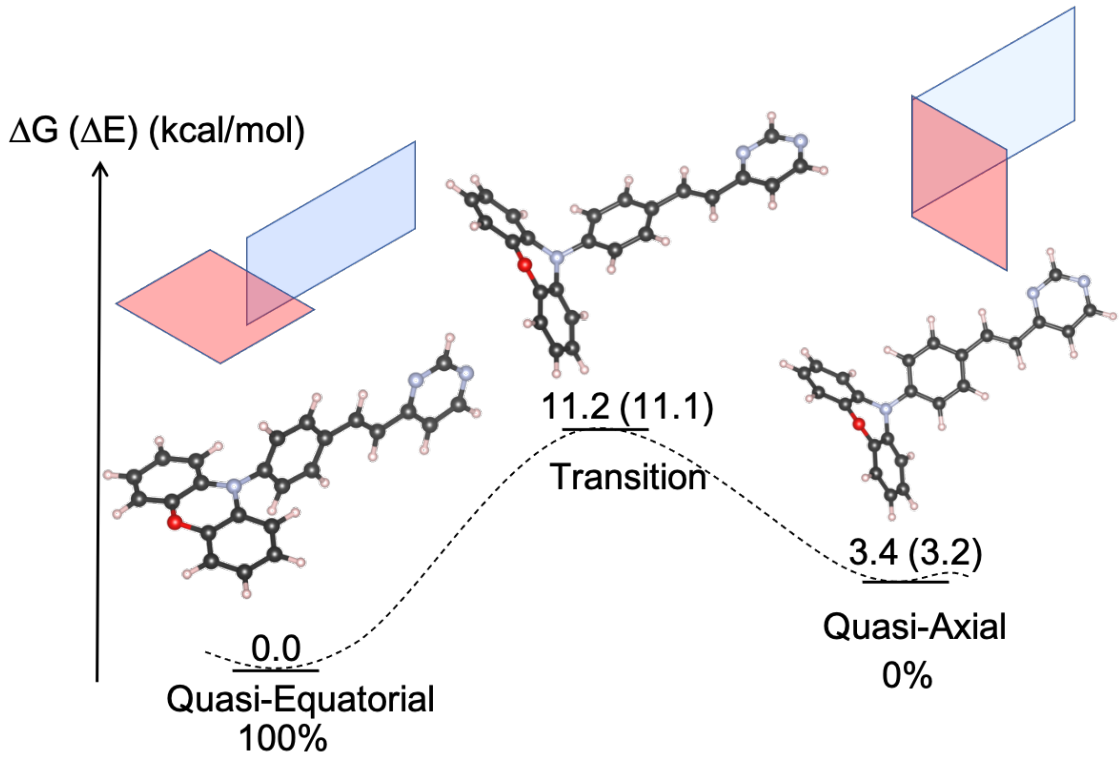

Figure S4: Relative total Gibbs free energies (total electronic energies in parenthesis) of the *Qeq* and *Qax* conformers and of the transition state, obtained at the ωB97X-D/6-311+G(d,p)

level of theory for compound **2**. Boltzmann relative populations obtained with ΔG are also presented.

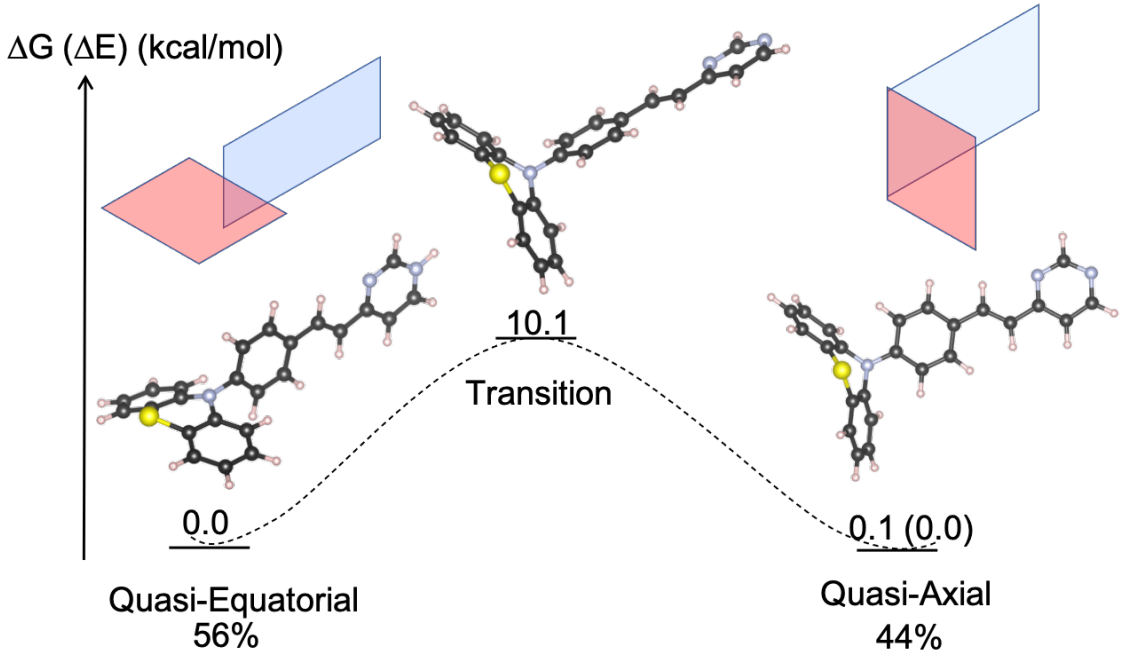

Figure S5: Relative total Gibbs free energies (total electronic energies in parenthesis) of the *Qeq* and *Qax* conformers and of the transition state, obtained at the ωB97X-D/6-311+G(d,p) level of theory for compound **3**. Boltzmann relative populations obtained with ΔG are also presented

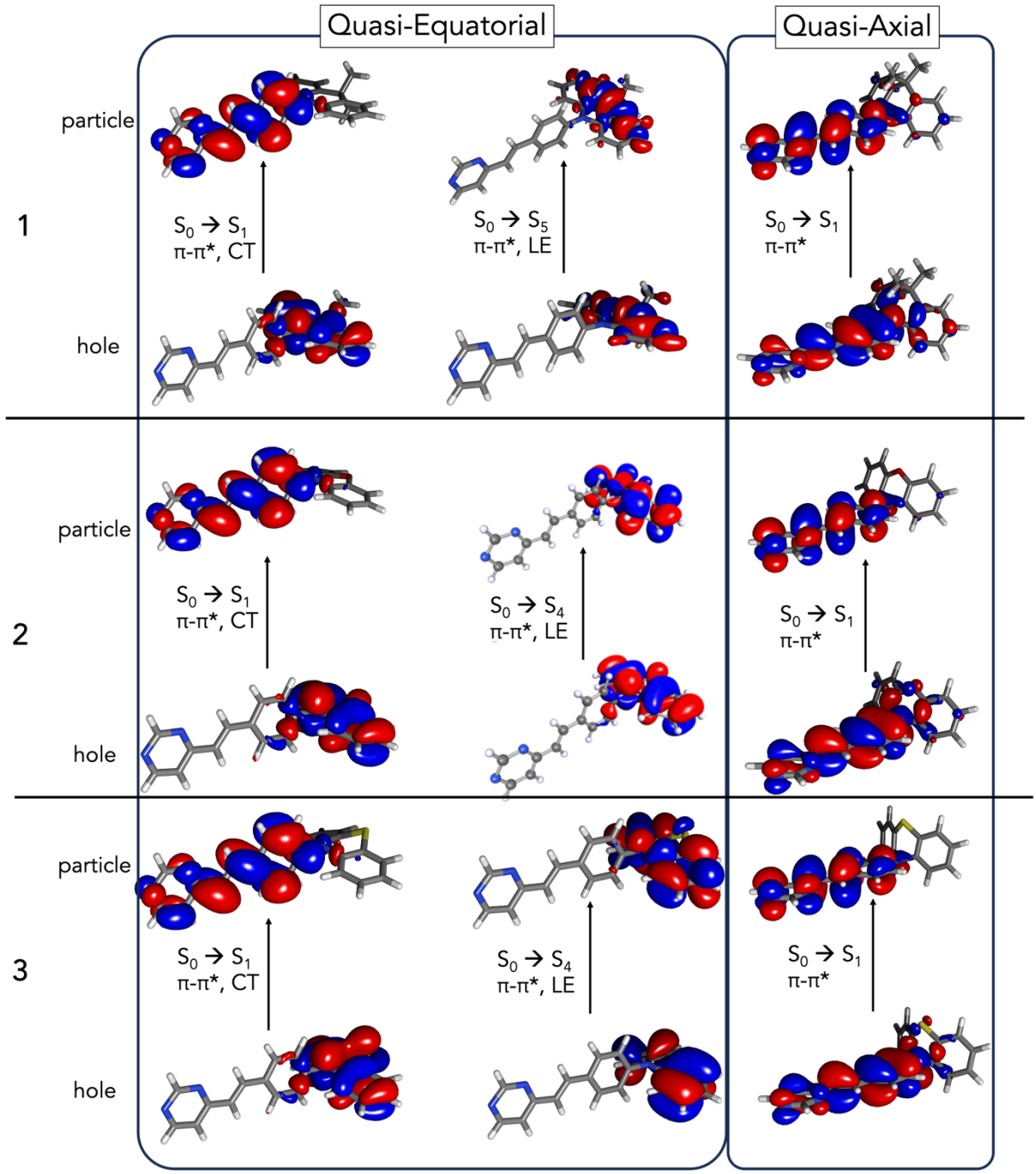

Figure S6: NTOs relevant to absorption of compounds **1-3**, computed at the SCS-CC2/def2-TZVP level in gas phase. (Isovalue = 0.02 $e^-/Å^3$)

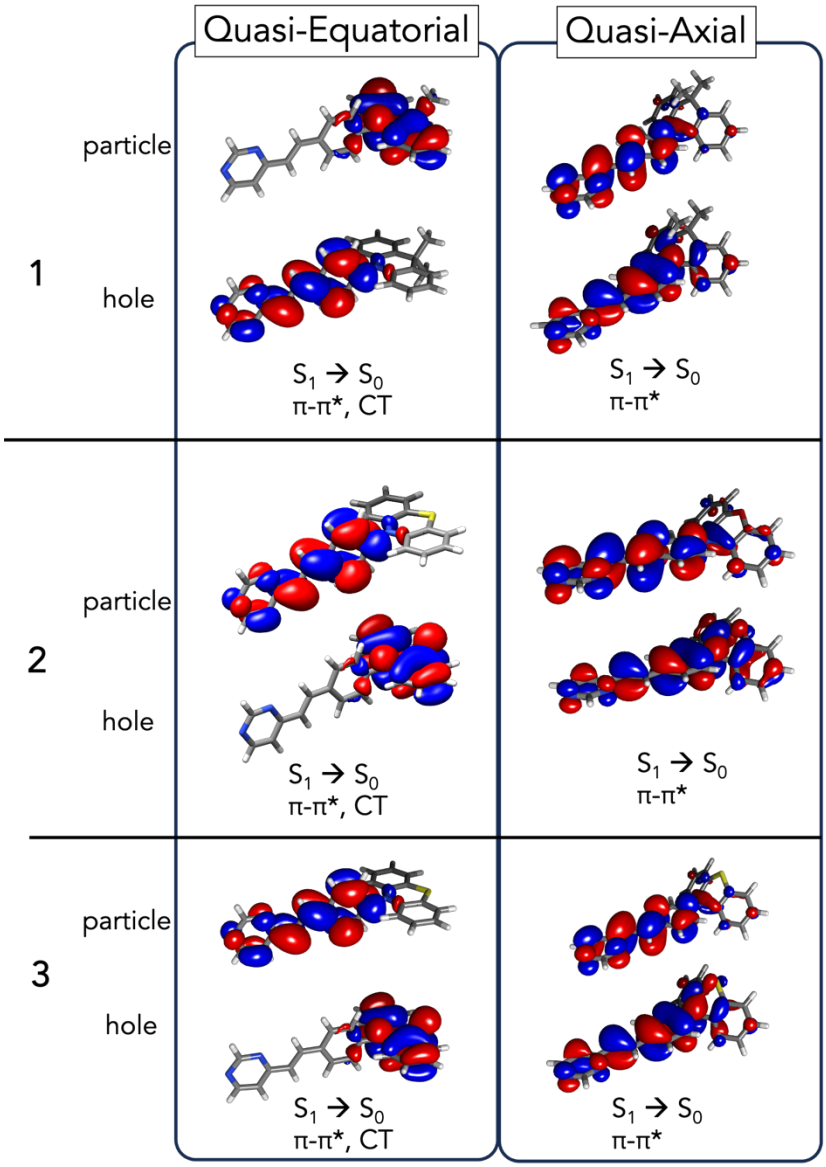

Figure S7: NTOs relevant to the emission of compounds **1-3**, computed at the SCS-CC2/def2-TZVP level in gas phase. (Isovalue = 0.02 $e^-/Å^3$)

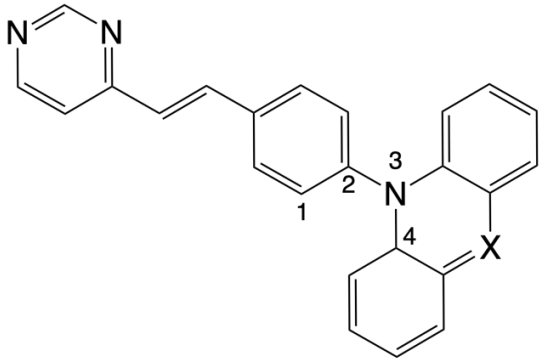

Figure S8: Atom numbering used in Table S1 to characterize the twist angle between the donor and acceptor in each of two conformers.

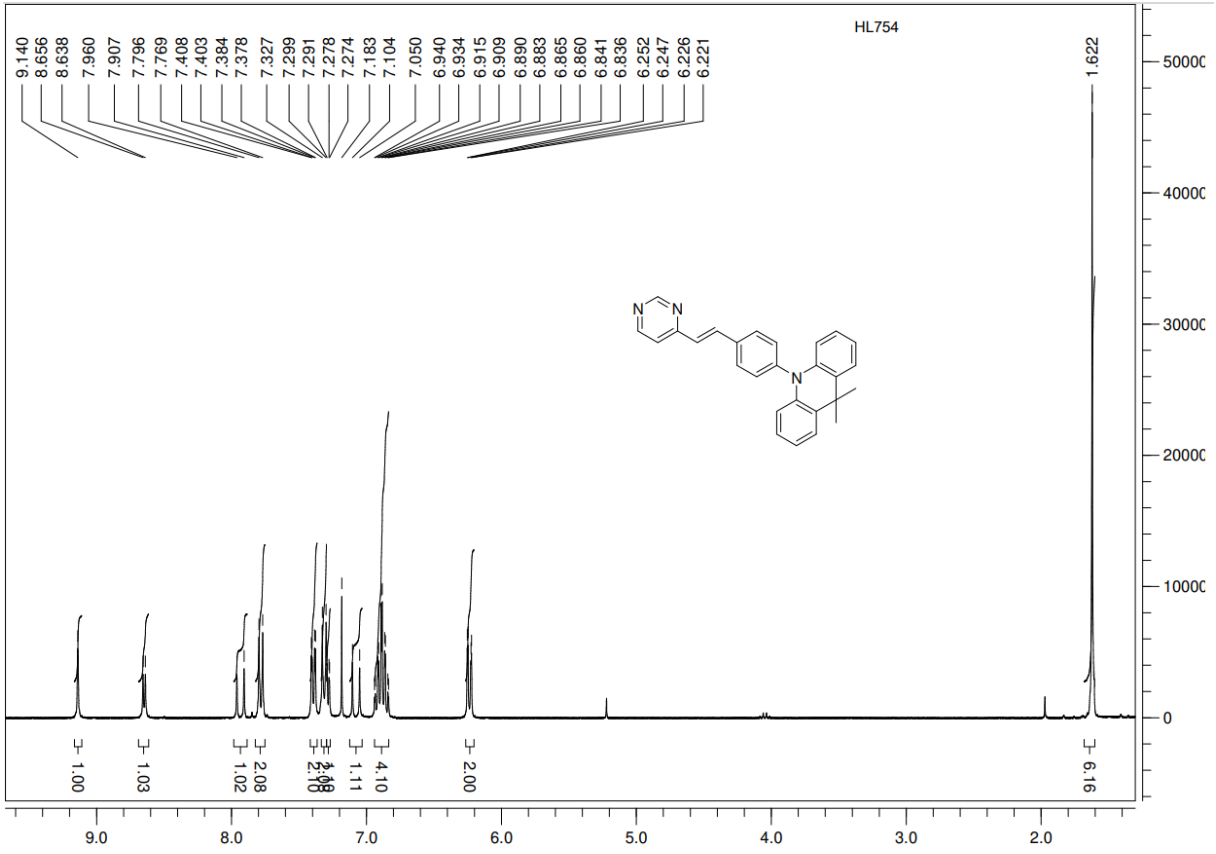

Figure S9: ^{1}H nmr spectrum (300 MHz) of **1** in $CDCl_3$

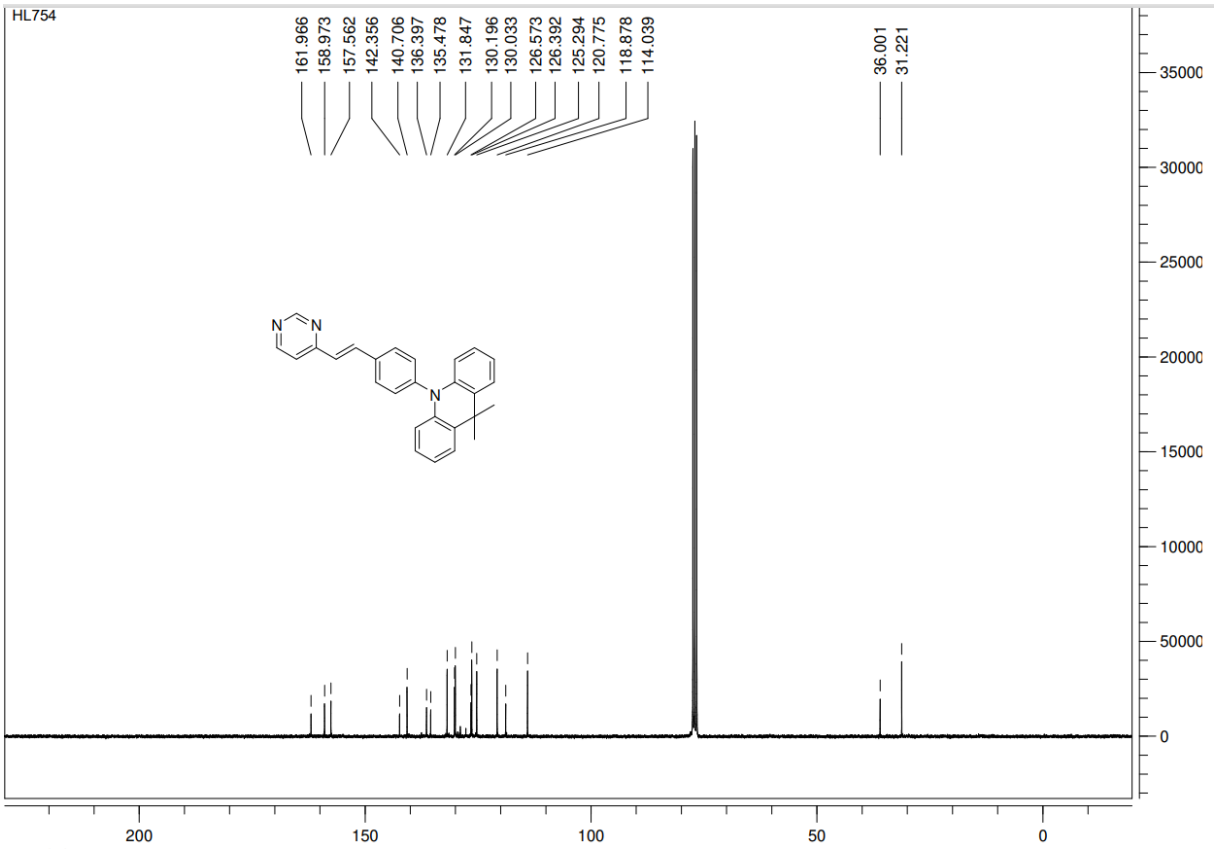

Figure S10: ^{13}C nmr spectrum (75 MHz) of **1** in $CDCl_3$

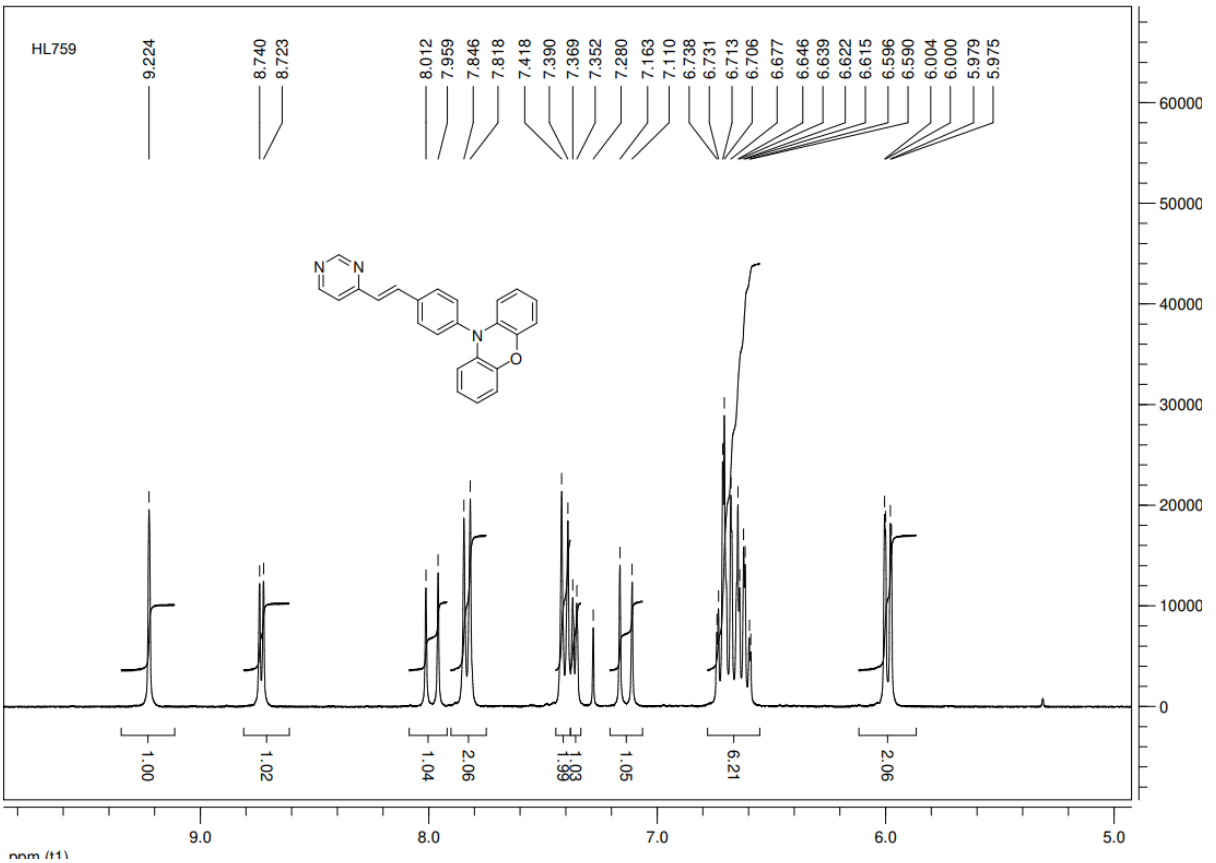

Figure S12: ^{1}H nmr spectrum (300 MHz) of **2** in $CDCl_3$

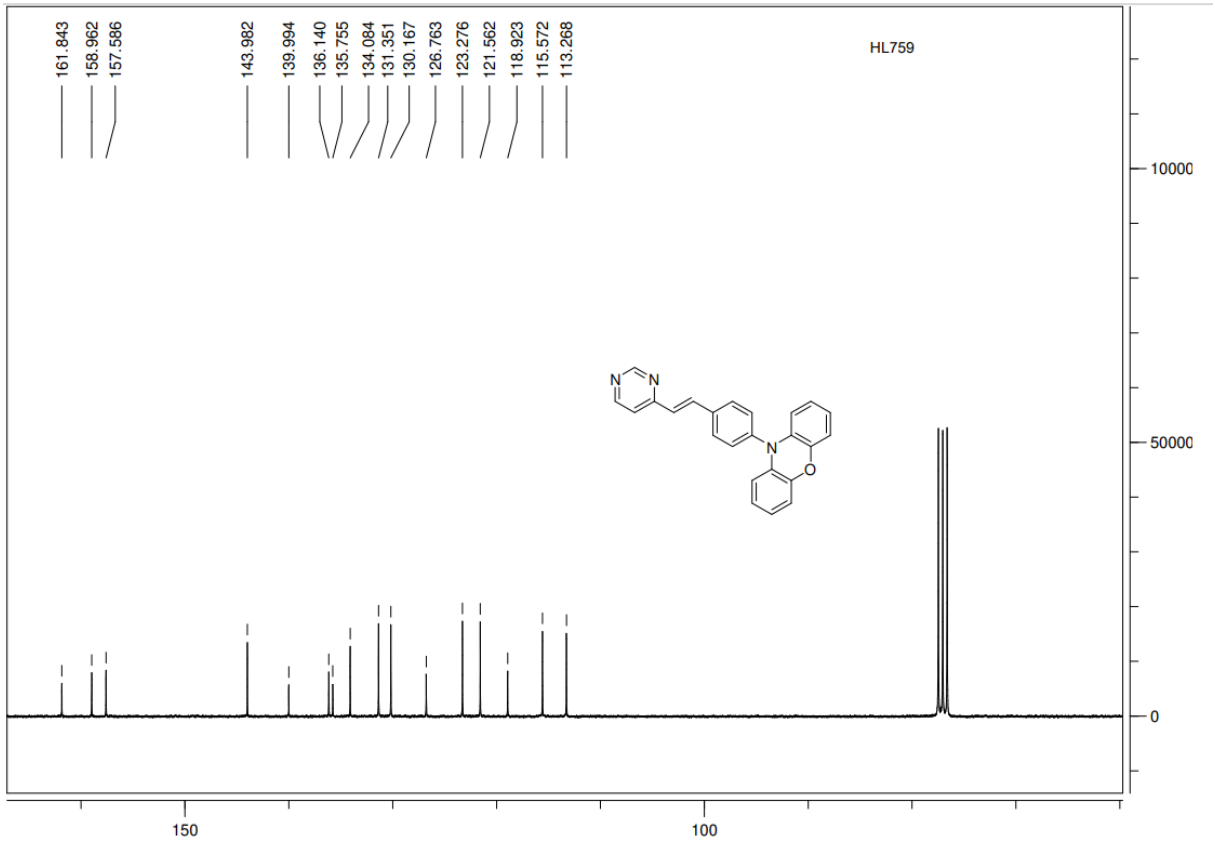

Figure S13: ^{13}C nmr spectrum (75 MHz) of **2** in $CDCl_3$

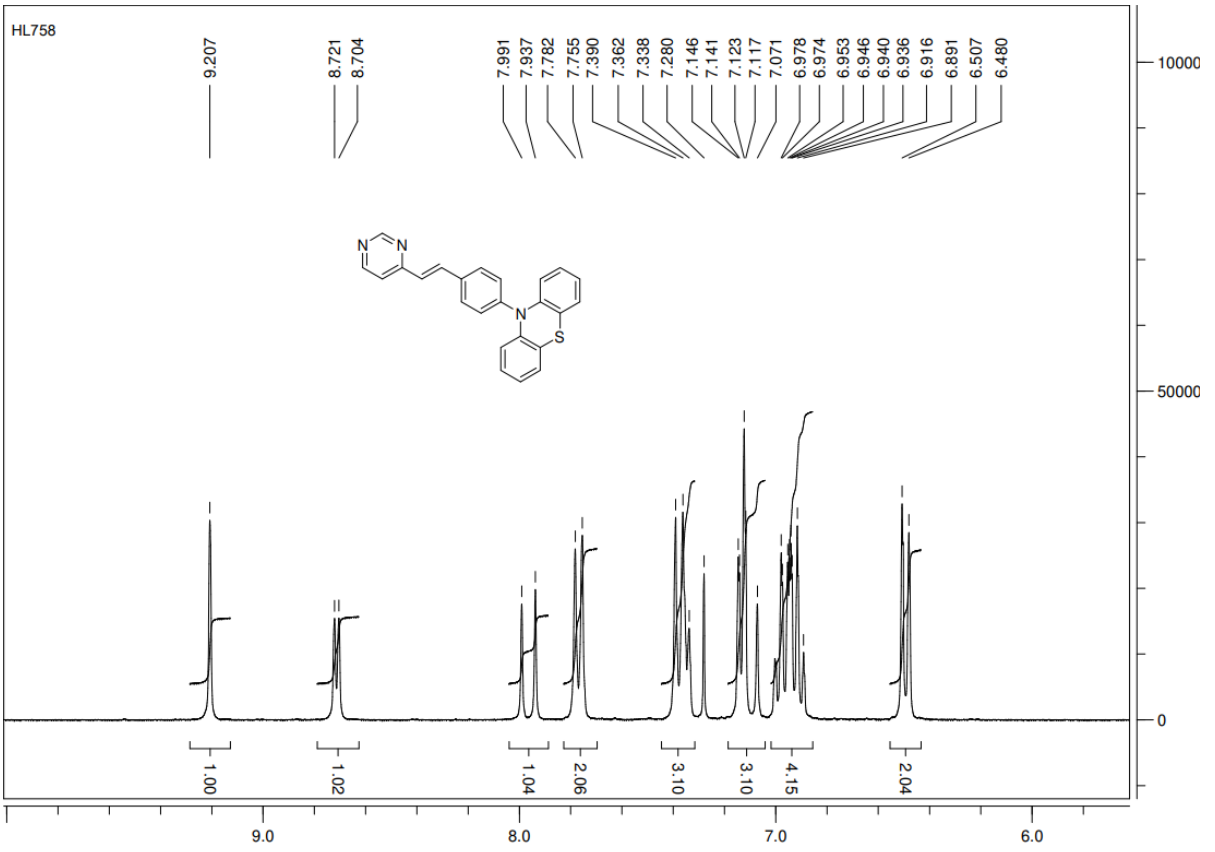

Figure S14: ^{1}H nmr spectrum (300 MHz) of **3** in $CDCl_3$

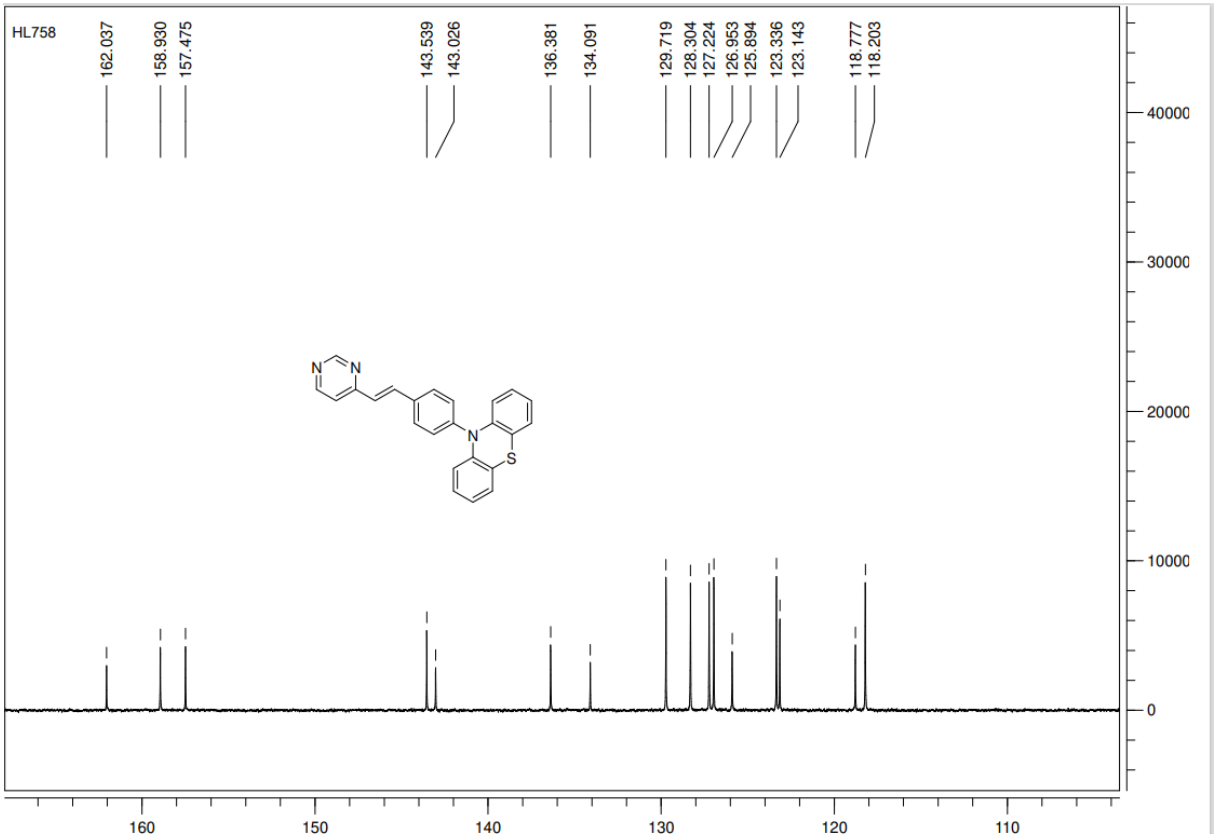

Figure S15: ^{13}C nmr spectrum (75 MHz) of **3** in $CDCl_3$